

## EXPERIMENTAL STUDIES RELATING TO MICROFRACTURE IN SANDSTONE

J.J. GALLAGHER Jr\*, M. FRIEDMAN, J. HANDIN and G.M. SOWERS

*Texas A and M University, Center for Tectonophysics, College Station, Texas (U.S.A.)*

(Accepted for publication May 11, 1973)

### ABSTRACT

Gallagher Jr, J.J., Friedman, M., Handin, J. and Sowers, G.M., 1974. Experimental studies relating to microfracture in sandstone. *Tectonophysics*, 21: 203–247.

A fundamental understanding of the relation between stress concentrations at grain contacts and microfractures in granular aggregates is obtained through two-dimensional photomechanical model studies and is tested through observational studies of experimentally deformed sandstone discs, glass beads, and quartz sand.

In uncemented aggregates, the state of stress in each grain is controlled by the manner in which the applied load is transmitted across grain contacts. The angles between lines connecting pairs of contacts and the axis of the principal load acting at the boundaries of the aggregate determine which of all contacts will be most highly stressed or "critical". Microfractures follow that maximum principal stress trajectory which connects critical contacts, and they propagate through those points where the magnitude of the local maximum stress difference is the greatest. Microfractures, therefore, are extension fractures. It then follows that both the locations and orientations of fractures can be predicted if the state of stress in the grains is known.

Positioning of critical contacts depends primarily on sorting, packing, grain shapes, and the boundary load conditions applied to the aggregate. Some critical contacts and, therefore, microfractures tend to join together in a series or "chain". Orientations of chains are most strongly influenced by the direction of the maximum compressive load at the boundary of the aggregate. A hydrostatic load applied on the boundaries of an aggregate can cause microfracturing within grains. Orientations for microfractures and contact lines are random in poorly sorted aggregates, but they are influenced by packing in well sorted aggregates.

Grains of cemented aggregates are more highly stressed at their centers than at contacts. By analogy, microfracture orientations depend strongly on the position of the greatest load axis and only slightly on the low-magnitude stress concentrations at contacts. These microfractures parallel the greatest principal stress trajectory in regions where the magnitude of the maximum stress difference is greatest. These observations lead to the conclusion that fractures in grains of cemented aggregates are also extension fractures and should exhibit a higher degree of preferred orientation than in uncemented counterparts.

These conclusions hold when cementing materials have about the same elastic moduli as the grains. Cements may be so weak that the aggregate behaves as if it were uncemented in terms of microfracture fabric, or so stiff that the major part of the load is transmitted by the cement, and the composite is no longer an aggregate in the mechanical sense.

---

\* Present address: Cities Service Oil Company, Exploration and Production Research, Tulsa, Okla., U.S.A.

## INTRODUCTION

The principal objective of this research is to gain an understanding of the relation between stresses in grains and microfracturing in granular aggregates. Local stress states are investigated in two-dimensional, resin analogs of loaded, granular rock aggregates such as sandstone. This research was undertaken to investigate and provide better understanding of the geological observation that there is a statistical correlation between the orientations of microfractures in grains and the stresses acting across the boundaries of the rock aggregate in bulk (Friedman, 1963; Hoshino and Koide, 1970). In addition, this study provides a better understanding of the manner in which boundary loads are transmitted from grain to grain through aggregates, how characteristics of an aggregate affect states of stress in grains and the mechanical effects of cementing on stress in grains.

The research is carried out in two phases, one dealing with uncemented and the other with cemented aggregates. Both types of aggregates are studied using a synthesis of photo-mechanics, experimental rock deformation, and petrofabrics.

Study of uncemented models was initiated with simple photoelastic arrays, culminating with a three-disc model. Stresses in this model are compared with fracture patterns in three rock discs. Similar comparisons are performed for larger arrays, some with circular and others with naturally shaped elements. Work on uncemented aggregates is concluded with petrofabric study of experimentally deformed glass spheres and unconsolidated quartz sand.

### *Previous work*

Ideas about fracturing of granular media often are based on the assumption that a uniform state of stress exists in the aggregate as a whole; thus, stresses in grains have not been considered in detail. A comprehensive review of the pertinent scientific and engineering literature has revealed that no detailed study of the state of stress in granular rock aggregates exists although related topics have been treated.

Stress solutions for idealized bodies under load, like discs or spheres loaded diametral-ly, are presented in most texts on the theory of elasticity (e.g., Timoshenko and Goodier, 1970). The exact solution for a single-line load on a cylinder was obtained by Poritsky (1950). None of these results has been applied to granular media. One reason for this is that states of stress in individual grains strongly influence the behavior of an aggregate within a limited range of conditions. These conditions lie between those traditionally studied in soil mechanics and in rock mechanics.

In soil mechanics, individual grains are assumed to be unbreakable. The deformations most frequently treated are in the form of either strain resulting from elastic deformations of grains with spherical shapes (Mindlin, 1954; Miller, 1963), ellipsoidal, cubical, and other shapes (Trollope, 1968), or failure of the bulk aggregate by unbroken grains sliding past one another in a plane (Rowe, 1962). Some of these situations have been investigated with the aid of photoelasticity (Dantu, 1968; Weber, 1968). These ap-

proaches are sufficient to describe the mechanics of granular media under the low-stress conditions commonly encountered in soil mechanics (Whitman, 1963; Rowe, 1964), but they are not adequate for rock mechanics. Grains in rock aggregates are usually constrained at higher confining pressures and by stronger, stiffer cements than normally exist in soils. As a result, the rock mechanist typically approaches the study of fracture by considering the stresses across the boundaries of an aggregate and then by neglecting contributions of individual grains to the behavior of the aggregate (Jaeger, 1966). The latter is an unwarranted simplification in that stress concentrations are observed photoelastically in both uncemented (Geertsma, 1963; Price, 1966, p.52) and cemented aggregates (Photoelastic Incorporated, 1970) analogous to rocks; and there is evidence that local states of stress affect the mechanical behavior of some rocks, e.g., fractures radiate from contacts in quartz grains (Borg and Maxwell, 1956).

It also has been demonstrated that microfractures are related to the orientations of the principal stresses acting across the boundaries of rock aggregates (Borg et al., 1960; Friedman, 1963; Hoshino and Koide, 1970; Gallagher et al., 1970a; Gallagher, 1971). Clearly, the behavior of an aggregate can be affected by the local states of stress that exist at and near grain contacts, especially when contributions from many grains are involved. The present study relates local states of stress in grains to both packing arrangement and boundary loads.

### *Experimental methods*

Lines of equal maximum stress difference and principal-stress trajectories are obtained for a variety of aggregates by use of standard photomechanical analysis. It will be shown that comparison of these states of stress with the loci of experimentally induced fractures in grains of rock aggregates permits development of a criterion to explain microfractures as extension fractures, i.e., a qualitative extension-fracture criterion. Similar comparisons were made at a larger scale for concrete and glass spheres by Arbiter et al. (1968). Their rock deformation experiments were dynamic and three-dimensional. The paths of fracture they observed followed theoretically derived  $\sigma_1$  trajectories (Fuchs, 1913) in areas of highest maximum stress difference as determined from two-dimensional photoelasticity. (See for explanation of symbols Notation I.)

Experiments on rock discs, natural quartz grains, and spherical glass beads are made to determine the extent to which the extension-fracture criterion applies.

### *Photoelasticity and model materials*

Photomechanical study is performed on models viewed in monochromatic green light with a 38-cm Chapman split-bench polariscope. Cemented and uncemented aggregate models of various sizes are deformed in an especially designed load frame. Uncemented photoelastic models are made of circular discs 2.5 cm in diameter and 0.6 cm thick or of "naturally" shaped elements (i.e., analogous in shape to sand grains), 2.5 cm maximum

## NOTATION I

Commonly used symbols are defined in the following list

---

- $N$  = frequency of contact lines
  - $N$ -chains = frequency of highly stressed (minimum fringe order = 1), connected contact lines
  - $m$  = frequency of microfractures
  - $m$ -chains = frequency of connected microfractures
  - $n$  = frequency of fringes (i.e., least fringe order) along all contact lines with a given orientation
  - $n$ -chains = frequency of total fringes for a chain of contact lines with a given orientation
  - $\theta$  = angle measured in any direction from the vertical load axis
  - $P$  = applied load.  $P_1 \perp P_2$ .  $P_1$  is arbitrarily chosen to act in a vertical direction.  $P_1$  is greater than  $P_2$  except where stated otherwise
  - $\sigma_1$  = greatest principal stress
  - $\sigma_2$  = least principal stress
  - Compression is positive; tension is negative.
- 

diameter. Low-magnitude thermal stresses introduced into model materials by cutting are negligible for the purpose of this study.

Initial work was performed with Columbia Resin (CR-39), which is easy to work with and is an ideal material for photomechanical work where great precision is not required. This material has the disadvantages of high creep rate and large time-edge effects; but neither of these disadvantages is great enough to vitiate our work. A polyester material, PSM-1, is used to verify results obtained with CR-39. The properties of PSM-1 allow more accurate measurements than with almost any other plastic that is commercially available (Photoelastic Incorporated, 1970). This material does not creep, has no time-edge effect, and is highly sensitive to small changes in applied load; however, PSM-1 is relatively expensive.

Discs of CR-39 and PSM-1 serve as the granular portion of cemented composite models. Several photoelastic cementing agents are used to bind the discs together. CIBA Araldite 520 epoxy with Triethylene Tetramine 951 hardener proves to be the easiest to use. CIBA epoxy has a Young's modulus of the same order of magnitude as both CR-39 and PSM-1.

Shell 815 epoxy with General Mills Versamid 140 hardener, Wards Bio-Plastic and catalyst, and William T. Bean RTC epoxy and activator are used to test results obtained with the CIBA Araldite. Models constructed with these cements confirm results obtained with CIBA Araldite.

### *Model construction*

Models of uncemented and cemented aggregates are constructed and deformed in containers made of plexiglass plates contained in a cold-rolled steel frame. The plates are so designed that they do not touch the array of discs, but if the array becomes unstable and collapses, the plates restrain the discs. Each part of the steel frame moves independently so that both vertical ( $P_1$ ) and horizontal ( $P_2$ ) loads can be applied to the aggregate.

All parts of cemented models are covered with layers of a suitable parting compound. The container is then half filled with liquid CIBA or other cementing material. Discs to be cemented together are submerged in the liquid cement and arranged in the desired configuration. The cement is then permitted to set up with the container walls in the horizontal position. After solidification of the cement, the container is removed, the initial state of stress due to cementing is recorded, and the model is deformed as desired.

Small magnitude stresses are introduced by the cementing process. These stresses are negligible with respect to the states of stress introduced into the model during deformation.

Photomechanics provides observations of detailed states of stress in a wide variety of model aggregates. States of stress in photoelastic models are evaluated through study of isoclinics (lines of equal orientation of principal stresses) and isochromatic fringes (lines of equal magnitude of maximum stress difference). These photoelastic data are collected using standard procedures (e.g., Frocht, 1941 and 1948). Comparisons of these observations with fracture patterns in experimentally deformed rock aggregates lead to the recognition of the relation between stress and fracture.

### *Experimental rock deformation*

Fractures are experimentally induced in rock discs, rock cylinders, glass beads, and quartz grains by two different testing techniques. Rock discs are fractured under unconfined, biaxial compressive loading conditions. Dry aggregates of glass beads and quartz grains and wet cylinders of cemented sandstone are deformed in triaxial compression.

Rock discs are biaxially deformed in the attempt to establish a relation between the state of stress and fracturing that permits prediction of either one from the other, i.e., a fracture criterion which can then be compared with models. The discs and chips of sandstone used in biaxial tests are fashioned from the same block of Tennessee Sandstone that was studied by Friedman and Logan (1970). Discs are mounted and deformed in the same containers used for photoelastic models. Only the steel loading members of the frame are in contact with the discs. Loading is terminated when the first fracture occurs.

The triaxial apparatus used is essentially the same as that described by Heard (1963). Tests are conducted at a strain rate of  $10^{-4}$  sec $^{-1}$ , under confining pressures to 1,000 bar, and dry specimens are axially shortened less than 20% at room temperature. The sensitivity of force measurements is  $\pm 2\%$ .

Sand-grain or glass-bead specimens are prepared by pouring the materials into annealed cylindrical copper jackets with a wall thickness of 0.02 cm and a diameter of 1.27 cm. The loose aggregates are tamped lightly to a porosity of 36–40%, i.e., to a non-cubic packing. Thin sections of this material, not otherwise deformed, show that no microfracturing is introduced into the specimen by tamping. End spacers isolate the specimen and, after deformation, permit separation of the specimen from pistons with minimal disturbance of the aggregate. Usually at least one of the end spacers is made of very porous fused silica to facilitate impregnation of the deformed aggregate.

### *Petrofabrics*

All microscopic data are collected from at least one hundred grains as viewed in a thin section cut along the cylindrical axis of each specimen. Before sectioning, the specimens are impregnated with Shell 815 epoxy while still in their copper jackets in order to preserve their fabric.

The orientation of the trace of contact lines and microfractures in individual "grains" in both photoelastic and experimentally deformed aggregates is expressed as the angle (designated  $\theta$ ) measured from the vertical external load axis (called  $P_1$ ). At  $\theta=0^\circ$  the trace of a contact line or microfracture is oriented parallel to  $P_1$ ; at  $\theta=90^\circ$ , the maximum value, the trace is perpendicular to  $P_1$  and parallel to the horizontal load,  $P_2$  (e.g., Fig. 11, p.215).

The frequency ( $N$ ) of contact lines and ( $m$ ) of microfracture traces are plotted as a function of  $\theta$  for the plane of each thin section. Corresponding data from photoelastic models are the frequency ( $N$ ) of contact lines as a function of the angle  $\theta$  and the frequency ( $n$ ) of fringes (i.e., least fringe order) observed along all contact lines with a given orientation.

For any one photoelastic disc, the line along which the least fringe order is greater than any other is regarded as a critical contact line, i.e., the line along which failure would occur in an analogous, isotropic, elastic grain. The contacts which are the end points of this line are called critical contacts. There is usually more than one critically stressed line in a photoelastic "grain", so that the orientations of all critically stressed lines are recorded, and all potential fractures are predicted.

Two-dimensional arrays of rock discs are treated the same as photoelastic models except that critically stressed lines are replaced by the traces of fractures in rock discs. Stresses in plastic discs are compared with fractures in rock grains to establish and evaluate the extension-fracture criterion.

## RESULTS

### *Uncemented aggregates*

Loads applied to the boundaries of uncemented aggregates are transmitted across grain contacts and through grains. The material responds initially by compaction in the form of rigid-body movements (Borg et al., 1960; Lee and Farhoomand, 1967, p.85). After a sufficient number of grain adjustments have taken place, a state of metastable equilibrium is reached in which all grains are constrained and rigid-body movements are prohibited. As the load continues to increase, all the deformation is elastic, both within grains and by reversible slip at grain contacts (Mindlin, 1949).

An aggregate with discontinuities between grains is statistically continuous in terms of stress if no grain movement is occurring, i.e., loads applied at one boundary are transmitted continuously from grain to grain to the other boundaries where, for static equilib-

rium, equal and opposite forces must be applied. In this sense, then, an aggregate may be treated as a continuum.

Stress concentrations arise at grain contacts in an aggregate because forces applied at the aggregate boundary are transmitted from grain to grain over small contact areas. Intensity of a stress concentration at a contact depends primarily on the size of the corresponding contact area and the orientation of the normal to that area relative to boundary loads.

The size of the contact area is a function of the forces at the contact, the mechanical properties of the grain materials, the size and the shape of the grains as well as other physical or chemical factors like "pressure solution." The attitude of a plane of contact depends on the size and shape of the grain and the arrangement of adjacent grains.

At some time in the loading history, the state of stress in a grain or group of grains can exceed the fracture strength of the material. The pattern of fractures thus formed in a grain depends on the same factors upon which stress concentrations depend.

If both boundary conditions acting on an aggregate and the characteristics of the aggregate and its constituent material are known well enough, then it is possible to describe in detail the state of stress in the aggregate. Generally, in a deformed rock, neither the boundary conditions acting on the rock nor the original nature of the aggregate at the time of deformation can be reconstructed. Knowledge of the state of stress in an aggregate at the time of deformation must be obtained by other means like observation of fractures that bear a known relation to stress concentration.

### *Three-disc model*

A three-disc model is a simple aggregate which serves to illustrate the above considerations in detail and to provide a basis for investigation of more complex models. Consider three photoelastic discs loaded as in Fig. 1. The vertical load is always made the

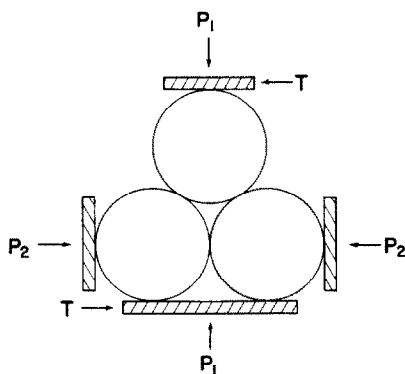


Fig. 1. Three-disc model configuration. Load  $P_2$  is sufficient to bring lower discs into contact with one another.  $P_1$  is then increased as desired. For some experiments a tangential load  $T$  is applied to the model.

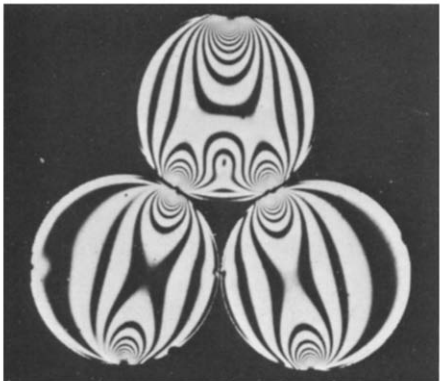


Fig. 2. Photoelastic fringes for a three-disc model. Loads are applied as in Fig. 1. The vertical load is  $570 \cdot 10^5$  dyn. Maximum stress difference on the first fringe, for example, is 50 bar. These CR-39 discs are 2.5 cm in diameter, 0.6 cm thick.

greatest. Usually, only normal boundary loads are applied to the model ( $P_1$  and  $P_2$ ); but one series of experiments does involve the application of a tangential force ( $T$ ).

For a photoelastic model subjected to normal loads only, the pattern and number of isochromatic fringes show the variations of intensity in maximum stress difference (or twice the maximum shear stress) within each disc (Fig. 2). The high number of fringes near contacts demonstrates the presence of stress concentrations (Fig. 3). These are usually expressed as stress concentration factors which, in the static case, are the ratio of

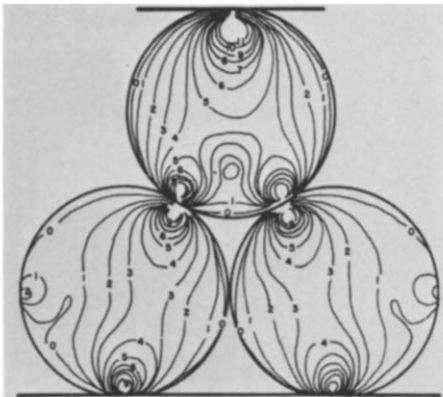


Fig. 3. Isochromatic fringe orders for a three-disc model. Vertical load is  $1,100 \cdot 10^5$  dyn. Each fringe represents about 50 bar maximum stress difference. Higher-order fringes near contacts are omitted. The highest fringe order in the model is 15 which occurs near the upper contact in the top disc. The magnitude of the maximum stress difference at that point is almost four times the stress at the upper contact. The stress-concentration factor for lower contacts in upper disc as well as at the most highly stressed contacts in lower discs is 3.

observed stress to nominal stress (i.e., the stress chosen as reference) at the point selected (e.g., Durelli and Riley, 1965, p.181). For convenience in photomechanics, this quantity can be expressed as the ratio of the observed fringe order to the force per unit area applied to the overall model, expressed in fringe orders. For example, in a model like that shown in Fig. 2, 21 fringes are counted with the aid of a microscope at the uppermost stress concentration. The stress at the uppermost contact is the force measured divided by the area of contact (Timoshenko and Goodier, 1970, p.409) which is 267 bar or about 5.3 fringes. Therefore, the stress concentration factor at this uppermost concentration is a little less than 4.

Similar computations show that the concentration factors at the lower contacts of the upper disc and at the most highly stressed contacts in the lower discs are about 3. Along the lines connecting contacts the concentration factor has a minimum value of about 0.5. The value of 4 at the uppermost contact is higher than at any other point in the model. These concentration factors may have some significance in determining where a fracture is most likely to initiate.

As the load on a model increases, the number of fringes at any point will also increase, but as long as static equilibrium is maintained, both the pattern of fringes and the stress concentration factor remain unchanged. Furthermore, all photoelastic materials subject to these same load conditions display the same fringe patterns although the number of fringes at any point may be different because it depends on the stress-optical characteristics of the material.

Isoclinics (Fig. 4), on the other hand, are not sensitive to changes of load intensity or to the material properties of the photoelastic model. Since isoclinic parameters (i.e., degrees clockwise rotation from horizontal and vertical) are related to the orientations of the principal stresses, they can be changed only by altering those conditions which govern the orientations of the principal stress trajectories in the model. Thus, isoclinic param-



Fig. 4. Zero-degree isoclinics for a three-disc model. Stress trajectories are vertical and horizontal at each point in the model where extinction occurs.

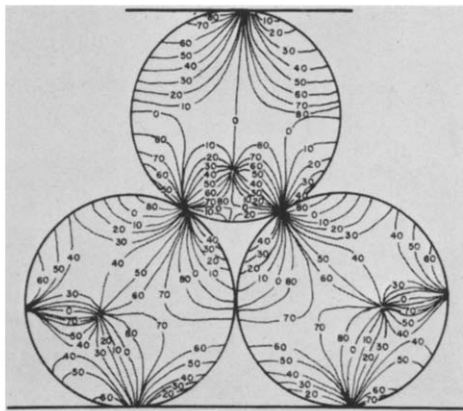


Fig. 5. Isoclinic parameters at  $10^\circ$ -increments for a three-disc model. Numbers indicate degrees of clockwise rotation in unison of the crossed polarizers from their originally vertical and horizontal positions.

eters, like fringe patterns and concentration factors, change only with the boundary conditions.

Study of all isoclinics for a particular model (Fig. 5) permits definition of the principal stress trajectories (Fig. 6). The principal stress trajectories for this three-disc model apply to any sort of elastic discs subjected to the same boundary conditions. If the discs are perfectly elastic prior to failure, then the relation between fracturing and the state of stress is determinable.

Application of a tangential force ( $T$  in Fig. 1) shifts the fringe patterns with respect to

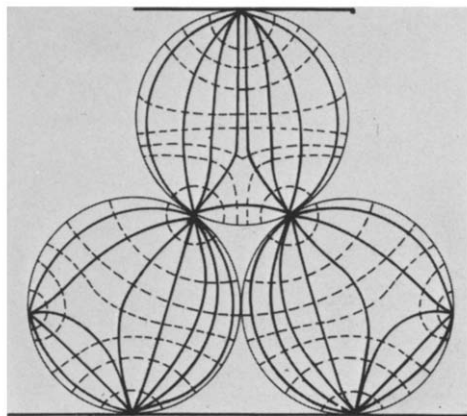


Fig. 6. Schematic of principal stress trajectories for a three-disc model. These plots are derived from isoclinic data (Fig. 5). The greatest principal stress trajectories are indicated by solid lines which also are extension fracture trajectories. Dashed lines indicate trajectories of the least principal stress.

their positions under normal loads, but there is very little difference in either the stress concentration factor or the positions of the isoclinics. The number of fringes increases on that side of the upper disc toward which the tangential force is acting. A similar situation is illustrated and discussed by Poritsky (1950, p.198).

#### *Loading of three rock discs*

Samples of Tennessee Sandstone are cut to the same dimensions as those of the photoelastic discs and loaded in the same three-disc configuration. Bedding, the main anisotropy in the rock, is parallel to the flat face of each disc. Each assemblage is loaded until fracturing occurs in at least one of the rock discs upon which the test is terminated. For discs of equal thickness the upper disc always breaks first; the lower ones do not fail (Fig. 7). This behavior is predictable from photoelastic data because the maximum stress difference in the central portion of the upper photoelastic disc is greater than that in the lower discs (Fig. 3), and the stress concentration factor at the upper contact of the disc is greater than at any point in either lower disc.

Fractures in the upper rock disc are observed to follow lines connecting contacts with the load frame and the lower discs. The path that fractures follow between contacts parallels the trajectories of greatest principal stress observed in the model analog, and it lies along the line which is the locus of the greatest values for maximum stress difference. Therefore, these fractures must be of the extension type.

Application of a tangential force to the upper loading plate ( $T$  in Fig. 1) results in a single fracture in the top rock disc. The position of this fracture is predictable from the photoelastic data for the new load condition. This single fracture forms on the more highly stressed side of the rock disc.

Using the foregoing information, one can predict the positions of fractures in the



Fig. 7. Fractures in the upper disc of an assemblage of three discs of Tennessee Sandstone. The top disc fractured at an applied load of  $280 \cdot 10^5$  dyn. All discs are 2.5 cm in diameter, 0.6 cm thick.

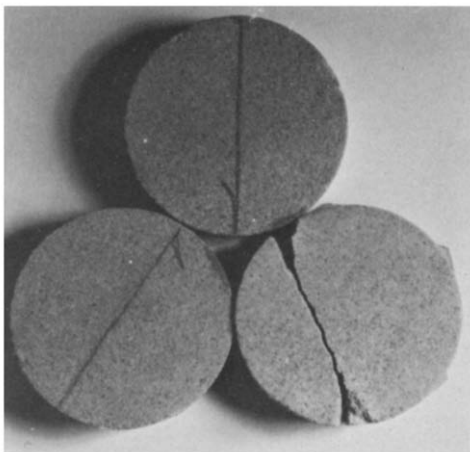


Fig. 8. Fractures in a thin lower disc of a three-disc assemblage. Lower right disc fractured at a load of  $250 \cdot 10^5$  dyn. applied to the top disc. The fractured disc is one-third the thickness of the others.

lower discs. The thickness of one lower rock disc is reduced to increase the magnitudes of stresses and to favor failure. The fractures that form follow the predicted paths (Fig. 8).

One result of experiments on three-disc assemblages is an overall predicted fracture array (Fig. 9). These experiments indicate a definite relation between stresses and fracturing, namely, fractures parallel  $\sigma_1$  trajectories in regions where the magnitude of the maximum stress difference is locally the greatest. Furthermore, this magnitude is greatest along critical contact lines. Thus, fractures tend to form along critical contact lines. This empirical relation is called "the extension-fracture criterion" because it is related to stress difference in elastic materials and, as will be demonstrated later, because it can be used to predict fracture locations and orientations in granular aggregates, given the stress condi-

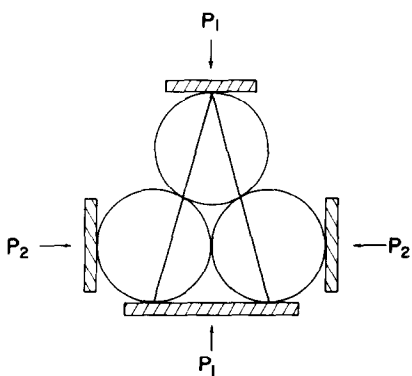


Fig. 9. Schematic for fracture trajectories for three-disc models. These fracture patterns are predicted from photoelastic data for  $P_1 \gg P_2$ , i.e., initially  $P_2$  is just sufficient to maintain contact between the two lower discs.

tions and vice versa. The word "extension" is used because the magnitudes of the principal stresses change from point to point along contact lines. Both principal stresses are compressive near contacts, although the least principal stress may change to tensile near the center.

#### *Loading large arrays of photoelastic discs*

It seemed likely that the extension-fracture theory could be extended to large arrays. However, application of the theory must be tested for changes in the states of stress within grains as a function of packing arrangement. Two were chosen for study, cubic and hexagonal (Fig. 10 and 11, respectively), and two-dimensional models were built up of photoelastic discs much as previously for the three-disc investigations. These arrays are the end members for the spectrum of possible packings for discs of equal size. They also represent two-dimensional slices through corresponding three-dimensional arrays (Graton and Fraser, 1935, p. 791). Each array is subjected to a variety of vertical and horizontal loads, and the resultant states of stress are examined.

Careful packing and loading of arrays leads to nearly uniform states of stress for all interior discs. Even when no particular care is taken to achieve nearly perfect packing, the

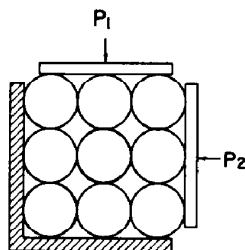


Fig. 10. Load configuration for cubic packing arrangement. If  $P_1$  and  $P_2$  are nearly the same magnitude, all discs are in contact with all their neighbors. If  $P_1 \gg P_2$ , then very little load is exerted across horizontal contacts and discs may not touch horizontally.

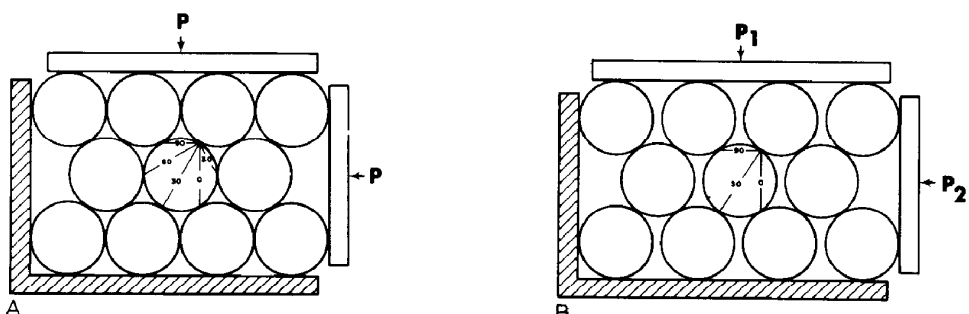


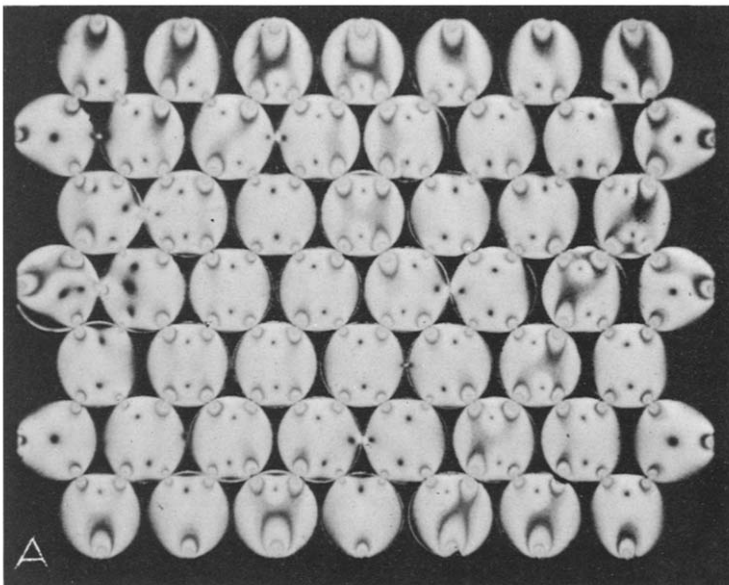
Fig. 11. Loading and packing configurations for idealized hexagonal arrays. Contact lines and  $\theta$  angles are depicted in the central disc of an array under uniform load  $P_1 = P_2 = P$  (A) and vertical load where  $P_1 > P_2$  (B).  $\theta$  angles are measured with respect to the vertical.

state of stress in any one inner disc is very much like that in its neighbors. Fringe patterns are essentially the same from one disc to another, although the number of fringes at corresponding points in any two interior discs varies by one or more (Fig. 12A). Zero-degree isoclinics display local variations, but the patterns for the aggregate as a whole are uniform (Fig. 12B). This high degree of uniformity is clearly visible in the consistently sinusoidal distribution of the 45° isoclinics (Fig. 12C). Therefore, study of the fringes and isoclinics in one typical inner disc should yield sufficient information to define statistically the state of stress in the aggregate of which it is a representative member.

Theoretically, there is a maximum of five possible fringe patterns for a typical interior disc in an ideally packed cubic array, three of which are shown in Fig. 13. Because of the symmetrical nature of cubic packing, the other two cases,  $P_1 < P_2$  and  $P_1 \ll P_2$ , are the same as  $P_1 > P_2$  and  $P_1 \gg P_2$  (Fig. 13b and 13c, respectively) but rotated 90°. Orientations for isoclinics that connect contacts for all five cases are the same as those of the lines connecting the contacts. Furthermore, the highest value of the maximum stress difference occurs along contact lines.

Application of the extension-fracture criterion to these photoelastic data allows prediction of likely fracture patterns for brittle analogs of typical inner discs subjected to each load condition (Fig. 13). The orientations of lines connecting contacts for each load condition are exactly at 0°, 45°, and 90° to  $P_1$  (Fig. 14a, 14e). The orientations of lines, along which the relative intensity of fringes is high, are restricted to these same angles for the cases of hydrostatic pressure ( $P_1 = P_2$ ) or extreme pressure difference ( $P_1 \gg P_2$ ).

The histograms showing the orientations of data for these idealized photoelastic



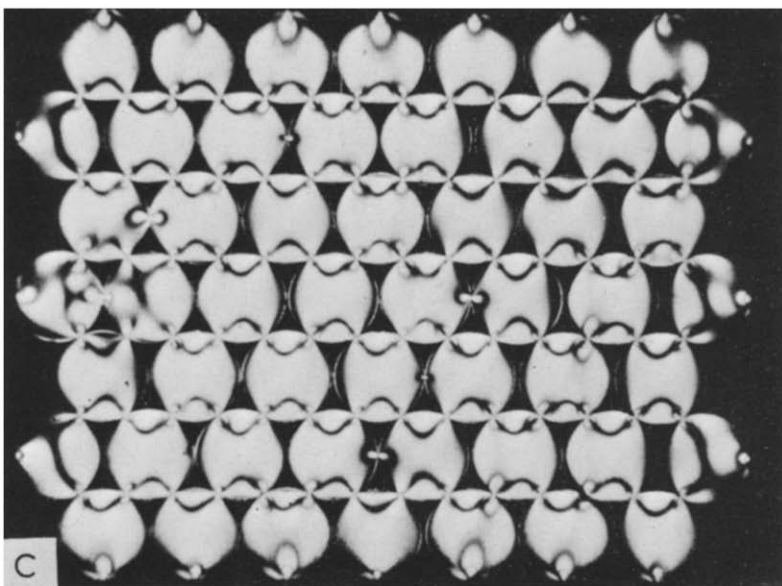
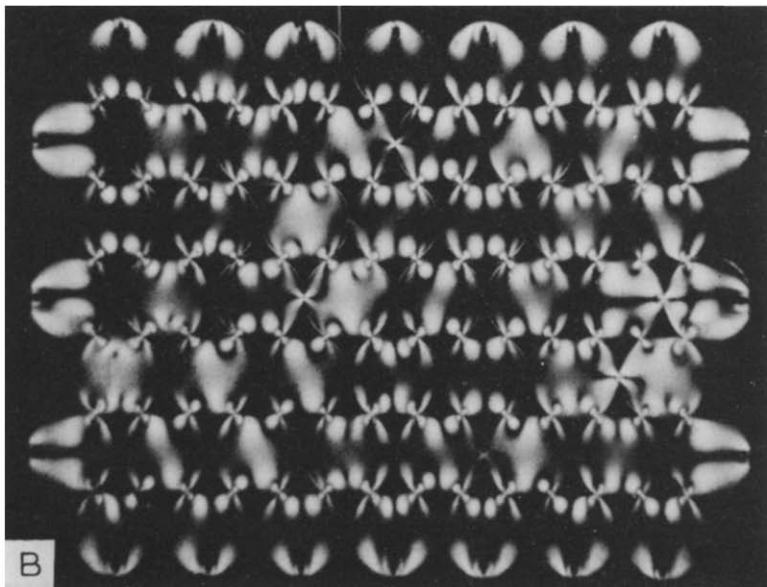


Fig. 12. Photographs of 52-disc photoelastic models. A. Isochromatic fringes. B. Zero-degree isoclinics. C. 45° isoclinics. Isoclinics are eliminated from A with quarter-wave plates.  $P_1 \gg P_2$ . The stress difference at the center of the top center disc is 30 bar.

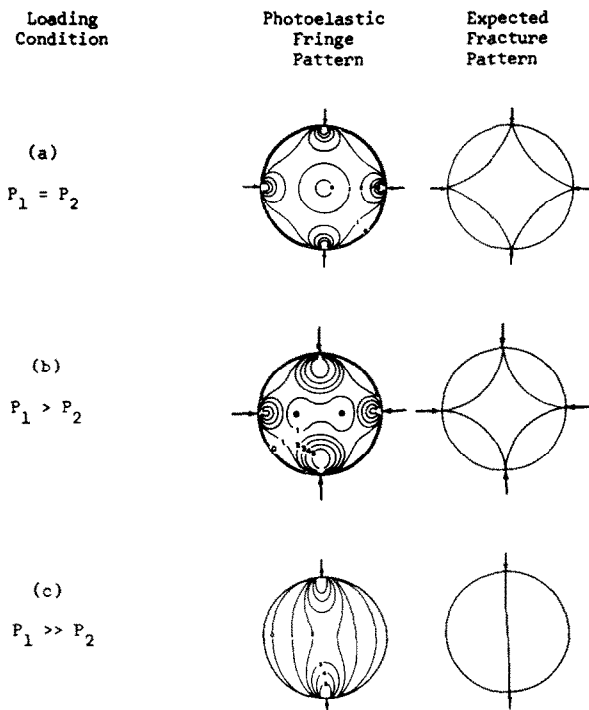


Fig. 13. Photoelastic fringes and expected fractures for typical inner discs in cubic arrays. Note the two isotropic points inside the first photoelastic fringe in the center of the disc shown in (b). ( $P_1, P_2$  are defined in Fig. 10).

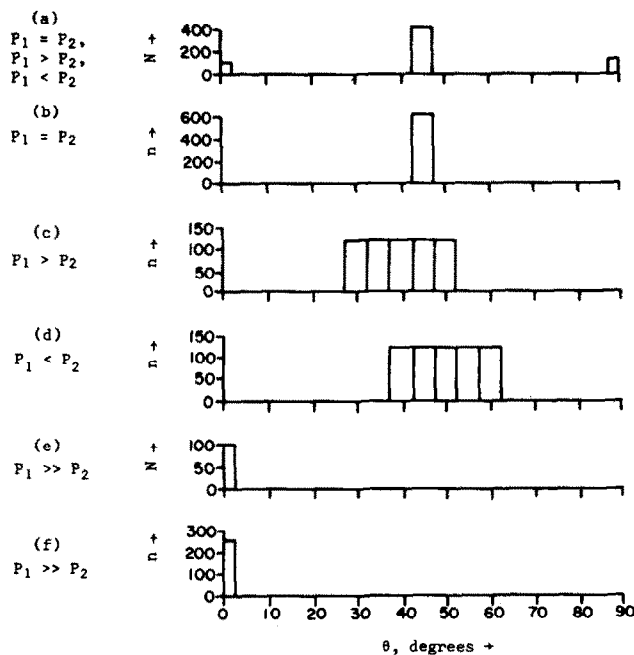


Fig. 14. Histograms showing  $N$  (a, e) or  $n$  (b, c, d, f) as functions of  $\theta$ . One hundred discs arranged in ideal cubic array loaded so that one fringe exists at the center of each disc. ( $P_1$  and  $P_2$  are defined in Fig. 10.)

models (Fig. 14) as well as those for other idealized models (Fig. 16, 17) are drawn arbitrarily with a 5°-spread of data that would be more typical of real, imperfectly packed aggregates. Changing the loading condition from  $P_1 \gg P_2$  to  $P_1 \ll P_2$  merely shifts  $\theta$  from 0° to 90°. The closer  $P_1$  and  $P_2$  are in magnitude, the wider is the spread of fringe orientations (Fig. 14c, 14d).

Orientations of contact lines and corresponding fringe orders for hexagonally packed arrays of discs are significantly different from those for cubic arrays (compare Fig. 13 and 14 with Fig. 15 and 16). Most noticeable are highly stressed contact lines near 30° and 60° to  $P_1$ . Photoelastic models with deliberately built-in random packing variations (Fig. 16f, 16g) are constructed so that possible limits for deviations from the orientations expected for perfect packing can be estimated. The results correspond well with their ideal counterparts (Fig. 16d, 16e), i.e., deviations rarely exceed a few degrees.

One obvious exception is the unexpectedly high fringe orders along horizontal lines (i.e. at 90° in Fig. 16). These lines are near edges of discs and they are more highly stressed than their ideal counterparts because the isotropic points, passed through by lines in the ideal case, have migrated to new positions. The result is that contact lines pass through the more highly stressed areas near the peripheries of discs in imperfectly ar-

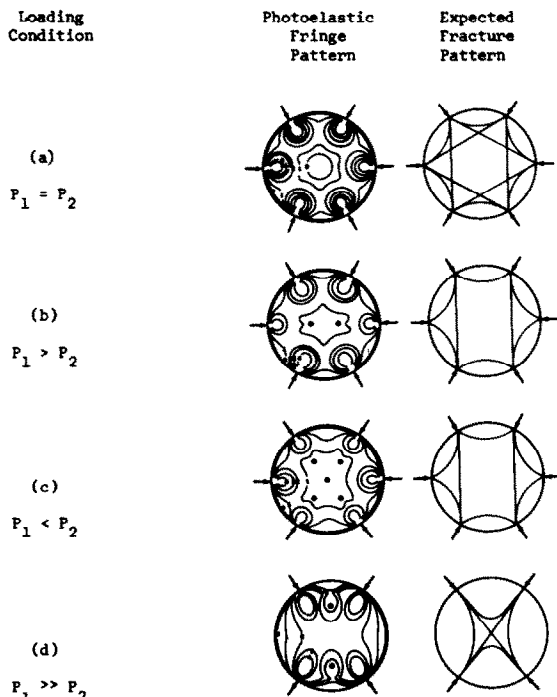


Fig. 15. Fringes and expected fractures in typical inner discs of hexagonal arrays. All six contacts with neighbors are significant influences on fringe patterns for (a), (b), and (c). The horizontal contacts are not significant for (d). Note the isotropic points inside the first fringe and near the center of (b) and (c) but near the edge of (d).

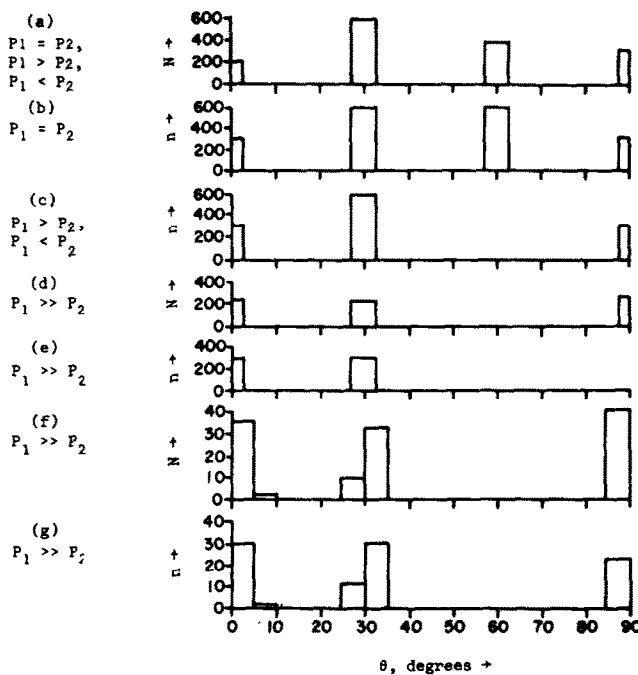


Fig. 16. Histograms showing  $N$  (a, d) or  $n$  (b, c, e) as functions of  $\theta$  for one hundred discs arranged in ideal hexagonal array and loaded so that one fringe exists at the center of each disc. Also patterns for thirty grains deliberately arranged in imperfect order (f, g).

ranged arrays. It follows then that microfractures in analogs to this array are most likely to have orientations distributed at  $\theta$  angles between  $30^\circ$  and  $60^\circ$  with some chance of occurrence near  $0^\circ$  and  $90^\circ$  (Fig. 17).

Photoelastic fringe patterns for individual discs in hexagonal arrays (Fig. 15) indicate that under analogous conditions, rock grains could display a variety of microfracture patterns. For discs in both cubic and hexagonal arrangements, as the number of contacts increases, the highly stressed areas migrate toward the edge of the disc; in analogous rock grains fractures would tend to become peripheral. For example, compare fracture patterns and corresponding fringe displays which penetrate grain interiors (Fig. 13c or 15d) with peripheral patterns for which the centers of discs and grains are very nearly isotropic (Fig. 13a, 13b, 15a, 15b, 15c). In general, however, the isochromatics for cubic and hexagonal arrays are easily distinguishable by both the number of stress concentrations and differences in fringe patterns. Corresponding fracture patterns are likewise readily distinguished.

#### *Experiments on glass beads*

The regularity and reproducibility of photoelastic fringe patterns, and hence of expected extension fracture orientations, in models of both cubic and hexagonal packing

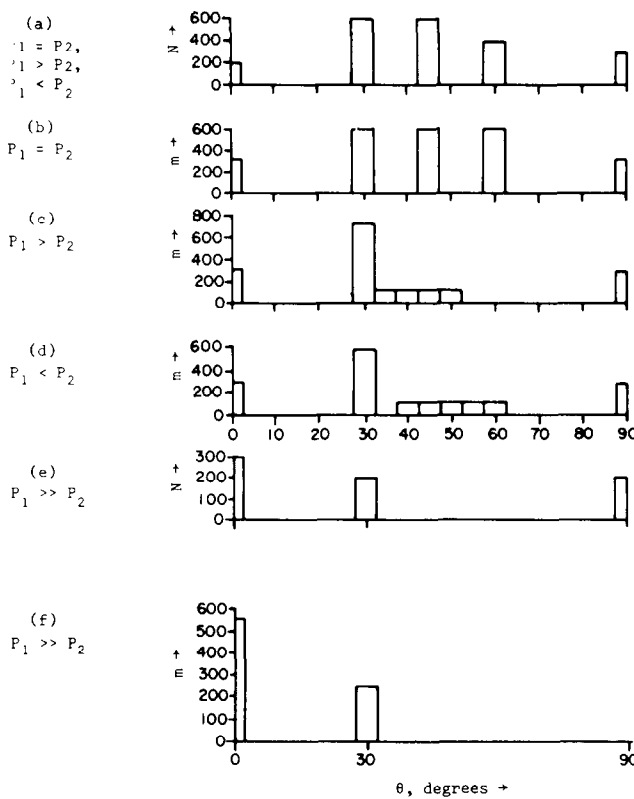


Fig. 17. Histograms showing  $N$  (a, e) or predicted  $m$  (b, c, d, f) as functions of  $\theta$  for two hundred discs arranged so that half the discs scattered randomly throughout the model were in contact with four neighboring discs and the other half in contact with eight neighbors.

suggested the next step of the investigation: study of fracturing in three-dimensional, loose aggregates of glass beads in triaxial compression. Here the grains consist of a material with different elastic properties; the beads are two orders of magnitude smaller in size than the photoelastic discs; and the aggregate is three-dimensional so that individual beads can be loaded along any direction. The system is still relatively simple, however, because the glass beads are all spherical, and the grain size can be controlled. Glass beads are Type A, Class 1 "microbeads" obtained from Microbeads Incorporated, Toledo, Ohio (T.J. Parker, personal communication, 1970).

The experimental data for aggregates of beads are tabulated in Table I. During application of the confining pressure audible snapping occurs and becomes frequent above about 350 bar. Thin sections of specimens which were deformed under confining pressure alone show that the snaps represent microfracturing in the beads, i.e., fracturing restricted to individual beads or grains (experiments 9, 24, 26, 27, 28 in Table I). Similar results are obtained for axially shortened specimens. At 350 bar confining pressure and about 6% strain (experiments 3, 5, 6, 7 in Table I) few grain fragments are observed in pore spaces

TABLE I

Experimentally deformed glass spheres

| Experiment number | Average grain size (mm) | Confining pressure (bar) | Shortening at termination (%) | Ultimate strength* <sup>4</sup> (bar) | Original specimen length (cm) |
|-------------------|-------------------------|--------------------------|-------------------------------|---------------------------------------|-------------------------------|
| 1                 | 0.6* <sup>1</sup>       | 170                      | 3.1                           | 350                                   | 2.54                          |
| 2                 | 0.6                     | 170                      | 3.2                           | 290                                   | 2.54                          |
| 3                 | 0.6                     | 350                      | 3.0                           | 290                                   | 2.67                          |
| 4                 | 0.3* <sup>2</sup>       | 350                      | 2.8                           | 360                                   | 2.84                          |
| 5                 | 0.6                     | 350                      | 6.0                           | 690                                   | 2.54                          |
| 6                 | 0.3                     | 350                      | 6.3                           | 430                                   | 2.56                          |
| 7                 | mixed* <sup>3</sup>     | 350                      | 6.4                           | 670                                   | 2.44                          |
| 9                 | 0.6                     | 350                      | 0.0                           | —                                     | 2.54                          |
| 15                | 0.6                     | 1,000                    | 12.8                          | 910                                   | 2.54                          |
| 17                | 0.6                     | 1,000                    | 17.7                          | 2,500                                 | 2.03                          |
| 18                | 0.6                     | 1,000                    | 13.9                          | 3,600                                 | 2.03                          |
| 19                | 0.6                     | 1,000                    | 12.6                          | 1,300                                 | 2.03                          |
| 20                | 0.6                     | 1,000                    | 15.2                          | 1,500                                 | 2.03                          |
| 21                | 0.3                     | 1,000                    | 7.3                           | 1,600                                 | 2.03                          |
| 24                | mixed                   | 1,000                    | 0.0                           | —                                     | 2.03                          |
| 26                | 0.6                     | 1,000                    | 0.0                           | —                                     | 2.57                          |
| 27                | 0.6                     | 1,000                    | 0.0                           | —                                     | 2.57                          |
| 28                | 0.6                     | 1,000                    | 0.0                           | —                                     | 2.57                          |
| 29                | 0.6                     | 1,000                    | 7.3                           | 730                                   | 1.60                          |
| 30                | 0.6                     | 1,000                    | 10.2                          | 830                                   | 2.61                          |

All experiments are in compression at room temperature and strain rate of  $10^{-4}$  sec $^{-1}$ . All specimens were encased in cylindrical copper jackets and were about 1.27 cm in diameter. No specimen failed macroscopically.

\*<sup>1</sup> The size of large glass spheres ranges from 0.5 to 0.7 mm.

\*<sup>2</sup> The size of small glass spheres ranges from 0.25 to 0.35 mm.

\*<sup>3</sup> Mixed specimens consist of 50 wt.% each of large and small spheres.

\*<sup>4</sup> Maximum ordinate of stress-strain curve.

(e.g., Fig. 18) but at higher pressures near 1,000 bar, and higher strain near 20% (experiments 18, 29, in Table I) many crushed fragments are packed into pore spaces.

The stress-strain curves for axially shortened aggregates of glass beads show stress drops if all details of the force record are plotted (Fig. 19). Each stress drop occurs simultaneously with a loud snap in the specimen. These microseismic events, like those heard during the application of confining pressure, appear to be related to microfracturing and, perhaps, to rigid-body movements as well.

Microfractures in a glass bead (Fig. 18) that has been subjected to a triple load (Fig. 1) resemble the patterns in the three-disc rock models (Fig. 7, 8). Fig. 20 shows a typical fracture pattern in a bead packed in a cubic array. Note the similarity to model patterns of Fig. 13c. Other microfracture patterns suggest hexagonal packing and their similarity to model patterns of Fig. 15 is noted.

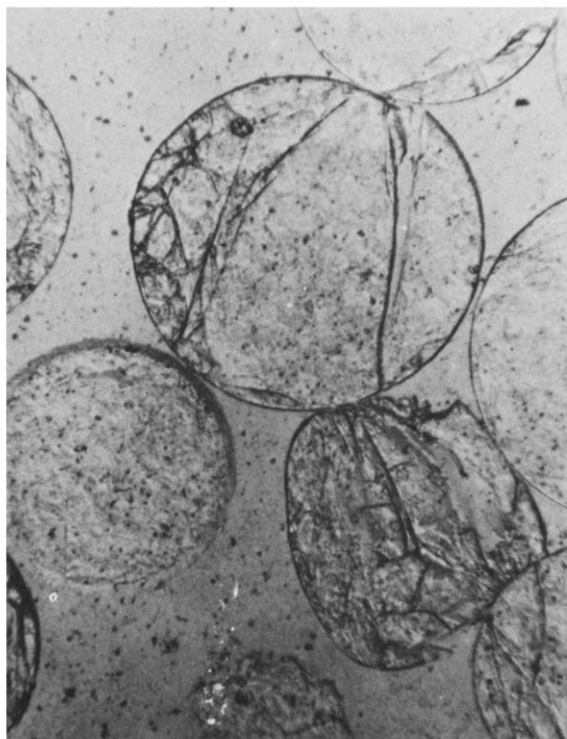


Fig. 18. Fractures in a glass bead which result from a triple load applied to the bead by its neighbors at 350 bar confining pressure. Upper bead is about 0.35 mm in diameter. (Experiment 6, Table I.)

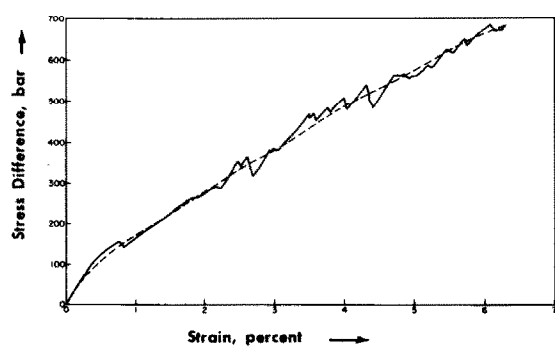


Fig. 19. Stress-strain curve for an aggregate of glass beads deformed at 350 bar confining pressure (experiment 5, Table I). The solid line shows numerous stress drops, each of which is accompanied by an audible snap. The dashed line is the average curve plotted by standard averaging conventions.

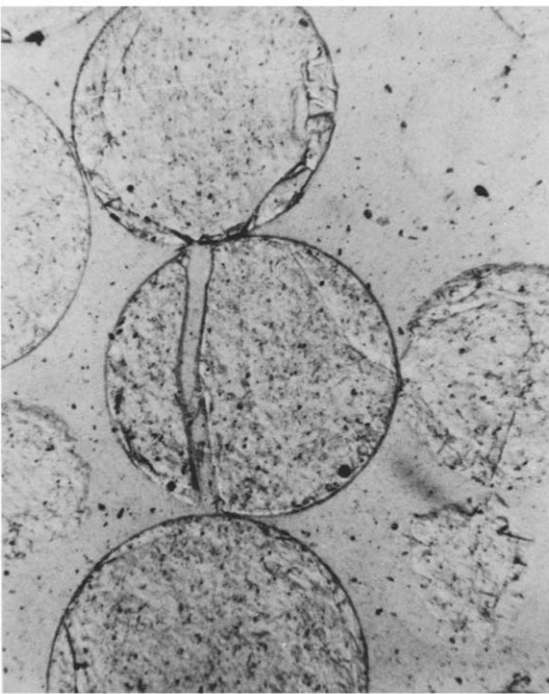


Fig. 20. A typical fracture pattern due to a diametral load on a glass bead deformed at 350 bar confining pressure. The major fracture in the central sphere probably resulted from one pair of critical contacts aligned subparallel to the greatest load and is probably in a cubic array. The greatest load was vertical. These beads are 0.3 mm in diameter.

Orientation data for contact lines and microfractures in aggregates of beads show certain significant trends. Cubic packing would be evidenced by concentrations within  $15^\circ$  of  $\theta = 45^\circ$  (Fig. 14). Contact lines and microfractures in this orientation occur for beads experimentally deformed at low confining pressures (Fig. 21a, 21b) but are noticeably less pronounced at higher confining pressures (Fig. 22). Hexagonal packing in models is reflected by the peaks near  $\theta$  angles of  $30^\circ$  and  $60^\circ$  (Fig. 16). Similarly oriented features occur in the beads (Fig. 21, 22, 23, 24), although displaced up to  $10^\circ$ . Models with combined cubic and hexagonal packings have highly stressed contact lines with a tendency to be preferentially oriented near  $\theta$  values of  $30^\circ$ ,  $45^\circ$ , and  $60^\circ$  (Fig. 17). Corresponding contact lines and microfractures are apparent in the deformed beads (Fig. 21, 22, 23, 24).

Some deformed aggregates of beads have high concentrations of contact lines and microfractures within a few degrees of  $\theta = 0^\circ$  (Fig. 22). These resemble concentrations of highly stressed contact lines in photoelastic models subjected to  $P_1 \gg P_2$  (Fig. 17e, 17f). Concentrations near  $\theta = 90^\circ$  (Fig. 21a) are expected from observations of photoelastic models under most pressure conditions (Fig. 17). When hydrostatic pressure is applied to glass-bead aggregates, or when the axial load is slightly less than the confining pressure, contact lines are somewhat more frequent and microfractures are very much more fre-

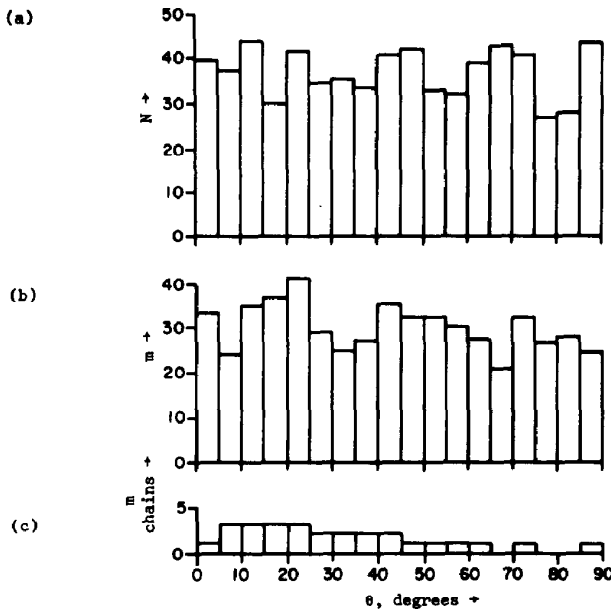


Fig. 21. Histograms showing  $N$ -(a),  $m$ -(b) or  $m$ -chains (c) as functions of  $\theta$  in an aggregate of 102 small spherical glass beads deformed at 350 bar confining pressure (experiment 6, Table I). There are 668 contact lines, 537 microfractures, and 27 chains. The chains tend to be preferentially oriented at angles between  $5^\circ$  and  $25^\circ$  and to a lesser extent between  $25^\circ$  and  $45^\circ$  to the direction in which  $P_1$  is acting.  $P_1 > P_2$ .

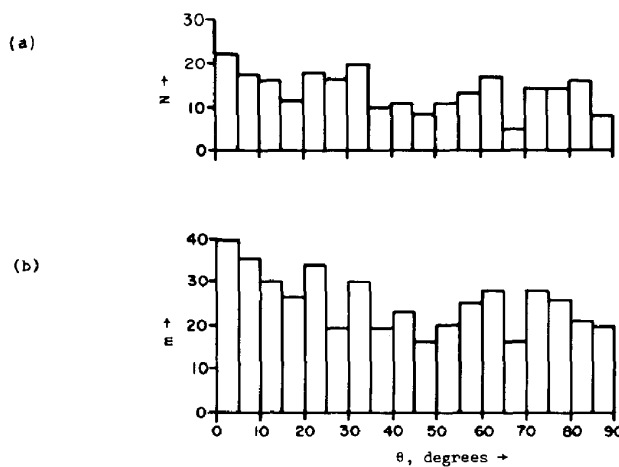


Fig. 22. Histograms showing  $N$  (a) or  $m$  (b) as functions of  $\theta$  in an aggregate of large glass beads deformed at 1,000 bar confining pressure (experiment 18, Table I).  $P_1 \gg P_2$ .

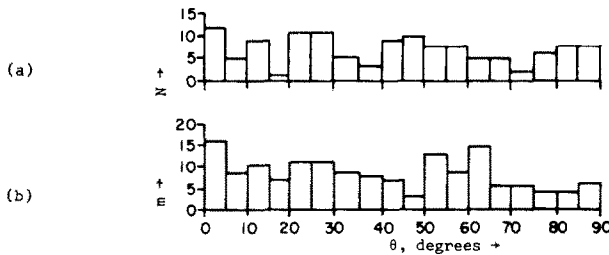


Fig. 23. Histograms showing  $N$  (a) or  $m$  (b) as functions of  $\theta$  in 100 grains of an aggregate of mixed glass beads deformed at 350 bar confining pressure (experiment 7, Table I). There are 136 contact lines and 160 microfractures.  $P_1 \gg P_2$ .

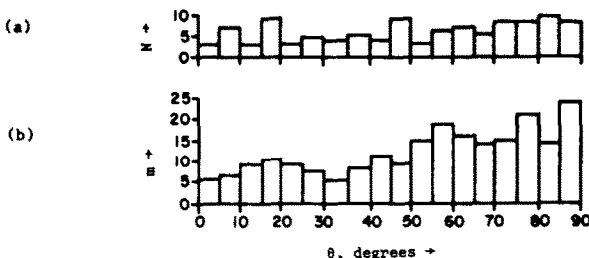


Fig. 24. Histograms showing  $N$  (a) or  $m$  (b) as functions of  $\theta$  measured with respect to the vertical ( $P_1 = P_2$ ) in an aggregate of 100 large glass beads deformed at 1,000 bar confining pressure (experiment 28, Table I). There are 108 lines and 226 microfractures. Note high concentrations near 90°.

quent between  $\theta$  values of 50° and 90° (Fig. 24). It is also apparent that contact lines are more uniformly oriented than are microfractures (compare Fig. 21a, 22a, 23a, and 21b, 22b, 23b, respectively). The frequency of microfractures tends to be slightly higher for  $\theta < 45^\circ$  (e.g., Fig. 22b). This preferential orientation permits the distinction between the greatest and the least load axes.

A final observation is that microfractures join together in a "chain". The chains provide an even better indication of the relative magnitude of the applied loads (compare Fig. 21b, 21c). However, chains involving three or more grains are rare. Only four chains could be counted on a section from experiment 5 (Table I), and only eight from experiment 18 (Table I).

#### *Models with naturally shaped elements of plastic and sandstone*

Tests on two-dimensional arrays of plastic and rock discs and three-dimensional arrays of glass beads demonstrated that the extension-fracture criterion is dependent on packing but independent of size and the material; the next variable studied was grain shape. The two-dimensional outlines chosen as representative of real sand grains are patterned after those in the St. Peter Sand.

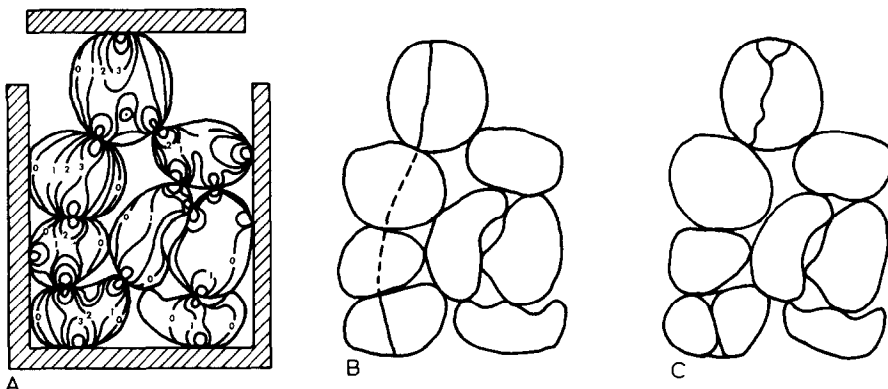


Fig. 25. Photoelastic fringes (A) and expected extension fracture orientations (B) in a model of eight naturally shaped elements of CR-39. The uppermost element is about 2.5 cm high. Also fractures actually observed in an identical assemblage of elements composed of Tennessee Sandstone (C). Failure is intentionally restricted to the upper and lowermost elements which are a little thinner than the others.

Two-dimensional photoelastic models composed of eight naturally shaped plastic elements are investigated (Fig. 25A) along with identical assemblages of elements composed of Tennessee Sandstone (Fig. 25C). Eight discs of CR-39 plastic are glued to rock discs, and both are simultaneously formed into the natural grain shapes on a lap plate. The finished products are unglued, separated, and the rock elements are arranged in the same fashion and subjected to the same load conditions as are the photoelastic elements. The locations and orientations of fractures experimentally induced in the rock are consistent with the extension-fracture criterion (compare Fig. 25B, 25C). Not all potential fractures occur in any one experiment because some rock elements are intentionally cut slightly thinner than the others and they break more easily. Furthermore, in uncemented aggregates once a grain breaks, the intensity of stress is locally reduced.

The locations and orientations of fractures seem to be predictable from these small arrays. To test this notion several large arrays of naturally shaped photoelastic elements were examined. The photoelastic display for a large array of naturally shaped elements shows that the state of stress in an aggregate is indeed complex (Fig. 26). Despite this complexity, six basic photoelastic patterns can be repeatedly identified (Fig. 27). The basic pattern resulting from one highly stressed contact (single load) and several contacts with very low stresses (Fig. 27a) occur more frequently than all other patterns combined. The magnitude of the maximum stress difference is relatively low compared to those for other patterns.

The isochromatic fringe displays in grains with two highly stressed contacts, i.e., one critical contact line (diametral loads), and displays for two critical contact lines that meet at one contact (triple loads) are familiar patterns in photoelasticity (Fig. 27b, 27c). They are also two of the most frequently observed patterns in arrays of naturally shaped photoelastic elements (Fig. 26B). They closely resemble the corresponding patterns observed in

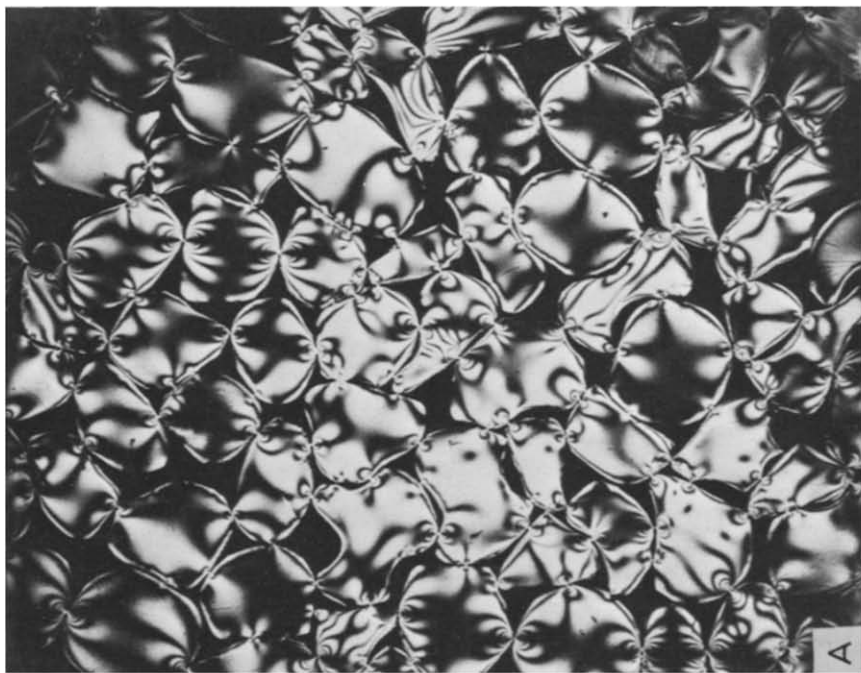
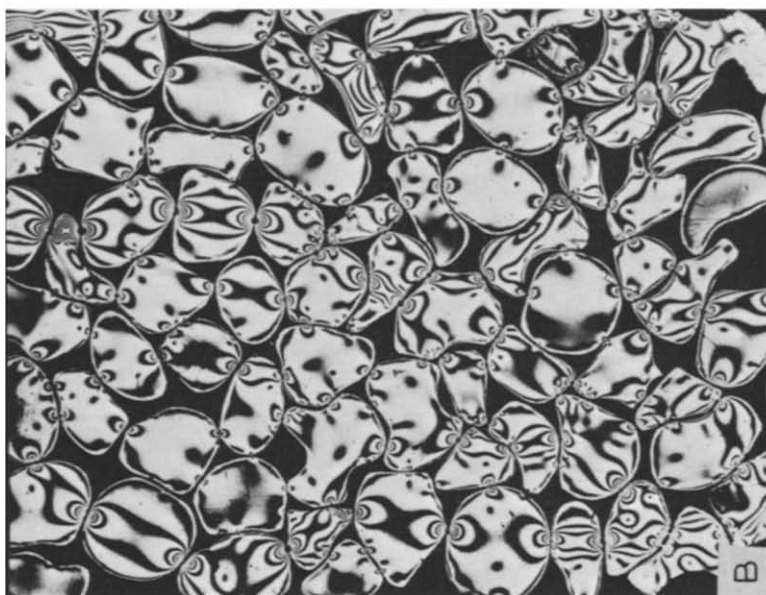


Fig. 26. Photoelastic display for CR-39 elements shaped to simulate rock grains. Discs are randomly packed. A. Zero-degree isoclinics are shown in plane light. B. Isochromatics are photographed in circularly polarized light.

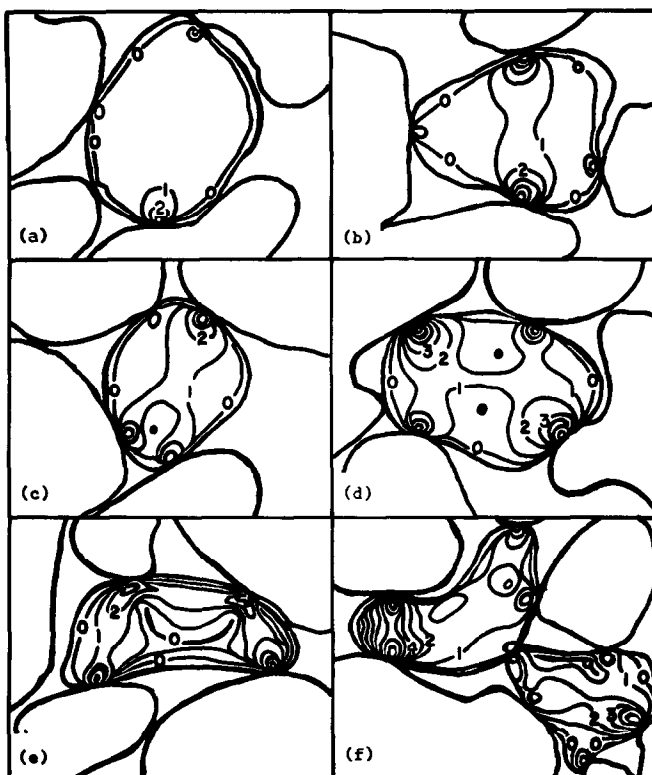


Fig. 27. Basic isochromatic patterns for naturally shaped CR-39 elements. Heavy lines represent boundaries. Light lines are isochromatic fringes. Each pattern represents a different load condition: (a) single load, (b) double or diametral load, (c) triple load, (d) quadruple load, (e) beam-like loads, (f) combined loads.

disc models. The isochromatics for naturally shaped elements highly stressed at two opposing contacts, are slightly distorted counterparts of those in a diametrically loaded disc (Fig. 13c). Furthermore, the critical contact line for such a pattern is a diameter that passes through the center of the circular stress pattern although it does not necessarily pass through the center of the grain. For these reasons, the load condition resulting in these fringe patterns is referred to as diametral. The triple load for a representative element (Fig. 27c) resembles a slightly distorted triple load pattern for a disc (Fig. 2).

Isochromatics for a quadruple load resemble those due to a pair of diametral loads placed next to each other, but connected at their midpoints (Fig. 27d). These fringes are similar to those in discs loaded at four contacts (Fig. 13a, 13b, 15d). The quadruple load is less common than diametral or triple but more common than beam-like loads (described below).

Photoelastic elements acting as beams display fringe patterns like those encountered for beams in engineering photomechanics. The bent elements even show a neutral fiber along which there is no maximum stress difference (Fig. 27e). The beam represents one of

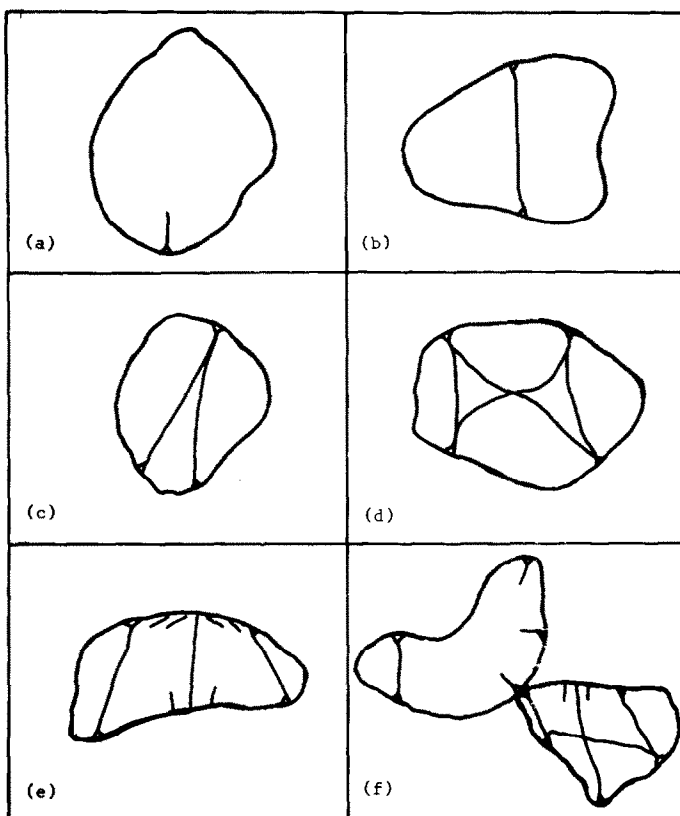


Fig. 28. Schematic for expected fracture patterns associated with basic fringe displays. Heavy lines are boundaries. Light lines are predicted fracture traces for a rock analog of photoelastic elements. Loads: (a) single, (b) double, (c) triple, (d) quadruple, (e) beam-like, (f) combined. Only those fractures that are considered to be most probable are shown in (e) and (f).

the simplest types of combined load configurations. Other combined loads are more complex and probably much more common in three-dimensional aggregates (Fig. 27f).

The expected fracture patterns associated with these basic fringe patterns are shown in Fig. 28 (compared with Fig. 27). For reasons to be discussed later, a single-load fracture is unlikely to transect a grain. For diametral loading, the maximum stress difference occurs along the straight line connecting contacts, and this same line is the predicted locus of extension fracturing. The triple-load fractures are slightly curved, but form a simple, easily identifiable pattern. The quadruple-load pattern is complicated and not as readily identifiable.

Which of the many potential fractures will eventually form in a bent grain depends upon the magnitudes of the loads applied at contacts and the positioning of these contacts. For example, the loading shown in Fig. 27e would probably result in one through-going fracture in the central region of the grain (Fig. 28e) due to the moments created by the nearness of the upper contacts relative to the lower. If the magnitude of the moments were reduced, and if all four contacts were equally loaded, then two subparallel diametral

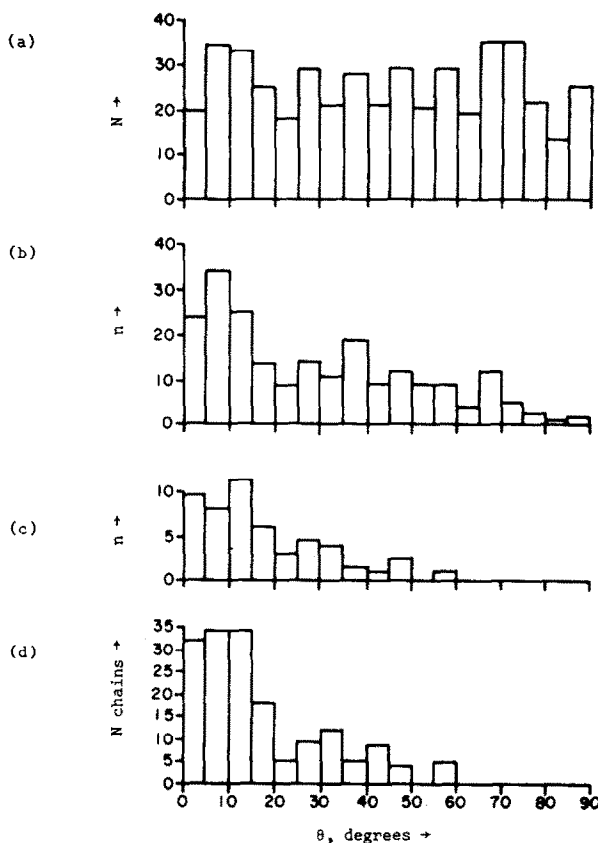


Fig. 29. Histograms showing  $N$  (a),  $n$  (b),  $n$ -chains (c), or  $N$ -chains (d) as functions of  $\theta$  for an array of sixty naturally shaped CR-39 elements. The vertical load is  $1.3 \cdot 10^8$  dyn. The model is constrained laterally so that most elements were in contact with horizontal neighbors prior to application of the vertical load.

fractures which resemble those predicted for the quadruple-load configuration would occur (compare Fig. 28d, 28e). Beam-loading has no counterpart in circular or spherical grains, and it is not likely that grains will have long unloaded central regions especially at high confining pressures. Combined loads could result in practically any fracture pattern. Fig. 28f depicts two possible patterns.

For two photoelastic models composed of naturally shaped elements the frequencies of contact lines are more or less uniformly distributed from  $\theta = 0^\circ$  to  $90^\circ$  (Fig. 29a, 30a). Contact lines at  $\theta$  values of  $50^\circ$  or less tend to be more highly stressed than those at  $\theta$  angles greater than  $50^\circ$  (Fig. 29b, 30b). Chains of contact lines are oriented at less than  $60^\circ$  to  $P_1$  and are more highly stressed at  $20^\circ$  and less for the larger of the two models studied (Fig. 29c, 29d).

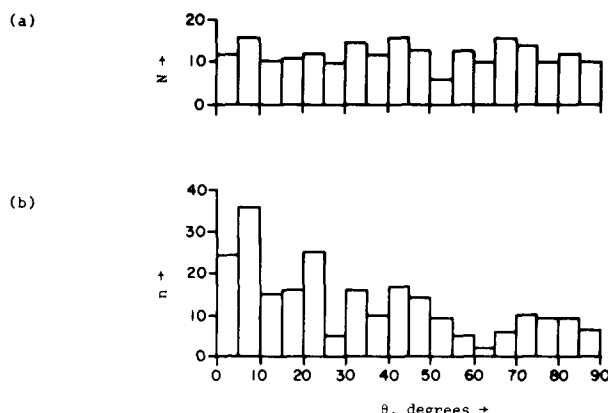


Fig. 30. Histograms showing  $N$  (a) or  $n$  (b) as functions of  $\theta$  for an array of 44 naturally shaped CR-39 elements. The vertical load is  $2.3 \cdot 10^8$  dyn and the horizontal load is about  $0.2 \cdot 10^8$  dyn.

#### *Tests on unconsolidated St. Peter Sand*

The last step in the investigation of the applicability of the extension-fracture criterion was the study of fracturing in triaxial experiments of uncemented aggregates of St. Peter

TABLE II

Experimentally deformed St. Peter Sand

| Experiment number | Average grain size (mm) | Confining pressure (bar) | Shortening at termination (%) | Ultimate strength <sup>*4</sup> (bar) | Original specimen length (cm) |
|-------------------|-------------------------|--------------------------|-------------------------------|---------------------------------------|-------------------------------|
| 8                 | 0.25 <sup>*1</sup>      | 350                      | 6.0                           | 500                                   | 2.54                          |
| 10                | 0.12 <sup>*2</sup>      | 350                      | 5.7                           | 440                                   | 2.67                          |
| 12                | mixed <sup>*3</sup>     | 350                      | 6.0                           | 400                                   | 2.54                          |
| 13                | 0.12                    | 350                      | 0.0                           | —                                     | 2.54                          |
| 14                | 0.12                    | 350                      | 5.4                           | 250                                   | 2.84                          |
| 16                | 0.25                    | 1,000                    | 0.0                           | —                                     | 1.45                          |
| 22                | 0.25                    | 1,000                    | 12.3                          | 2,500                                 | 1.52                          |
| 23                | 0.25                    | 1,000                    | 0.0                           | —                                     | 1.52                          |

All experiments are dry in compression, at room temperature and at a strain rate of  $10^{-4}$  sec<sup>-1</sup>. Specimens are mounted in copper jackets with fused silica and cold-rolled steel end spacers. Samples are about 1.27 cm in diameter. No specimen failed macroscopically.

<sup>\*1</sup> Size range is from about 0.21 mm to 0.30 mm.

<sup>\*2</sup> Size range is from about 0.10 mm to 0.15 mm.

<sup>\*3</sup> Mixed specimens consist of 50 wt.% each of large and small grains.

<sup>\*4</sup> Maximum ordinate of stress-strain curve.

TABLE III  
Experimentally deformed St. Peter Sand (after Borg et al., 1960, p.145)

| Experiment number | Grain size (mm) | Confining pressure (bar) | Shortening at termination (%) | Ultimate strength* <sup>2</sup> (bar) |
|-------------------|-----------------|--------------------------|-------------------------------|---------------------------------------|
| 379* <sup>1</sup> | 0.25 – 0.30     | 1,000                    | 10.6                          | 1,180                                 |
| 380               | 0.25 – 0.30     | 1,000                    | 15.5                          | 1,530                                 |
| 381               | 0.25 – 0.30     | 500                      | 21.6                          | 970                                   |
| 450               | 0.25 – 0.30     | 1,000                    | 3.0                           | 430                                   |

\*<sup>1</sup> All these specimens are compressed dry at room temperature and at a strain rate of  $10^{-4}$  sec<sup>-1</sup>.

None was brought to macroscopic failure.

\*<sup>2</sup> Maximum ordinate on the stress-strain curve.

quartz sand (Table II). Experiments were done on the same starting material used previously by Borg et al. (1960), and some of Borg's thin sections were examined for comparison (Table III).

Below about 350 bar confining pressure and at about 6% shortening (experiments 8, 12, 14 in Table II), only a few fragments are observed in the pore spaces, i.e., most of the shortening is accomplished by rigid-body rotations of grains. At 500 bar and larger shortening from 10 to 20% (experiments 22, 379, 380, 450 Tables II and III), pore spaces are filled with crushed material from demolished grains.

The orientations of microfractures in the quartz grains resemble those predicted from photoelastic models and those observed in deformed glass beads. Assuming that the extension-fracture criterion applies in the same manner to quartz grains, the following comparisons are made:

(1) Fracture patterns which result from triple loads (Fig. 31, 32) strongly resemble predictions for the upper element in three-disc models (Fig. 7 and 9), as well as fracture patterns in glass spheres (Fig. 18). This pattern is observed in grains with near-circular sections (Fig. 31, 32) as well as those with elongate sections. Fractures due to triple loads are one of the basic patterns predicted from photoelastic study of naturally shaped elements (Fig. 28c).

(2) Fractures due to diametral loads observed in sand grains are similar to those predicted from photoelastic study of the lower discs of the three-disc configuration (Fig. 9), of circular discs arranged in cubic arrays (Fig. 13c), and observed in rock discs (Fig. 8) and glass beads (Fig. 20).

(3) Patterns of fracture due to quadruple loads on quartz grains (Fig. 31) are reminiscent of those predicted from study of photoelastic models comprised of circular

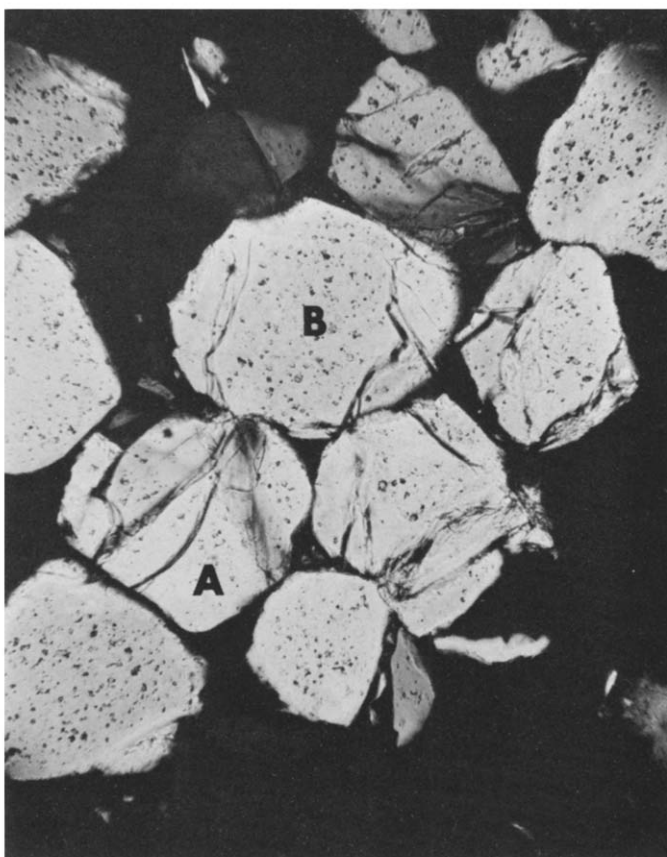


Fig. 31. Fractured quartz grains in St. Peter Sand. This is a photomicrograph of experiment 450 in which the material was deformed at 1,000 bar confining pressure (Table III). Grain *A* exhibits a fracture pattern due to a triple load. Grain *B* exhibits a fracture pattern due to a quadruple load.

elements packed in cubic arrays (Fig. 13a, 13b), hexagonal arrays (Fig. 15d), and for naturally shaped elements (Fig. 28d).

(4) More complex fracture patterns, like those for bent grains can also be related to photoelastic predictions (Fig. 28e, 28f).

(5) Chains of fracture like those seen in deformed glass beads are observed in deformed sand (Fig. 33). Chains connecting three or more grains were counted from thin sections for seven experiments (1, 12, 14, 22 in Table II, and 380, 381, 450 in Table III). An average of seven chains could be counted. Most of these are oriented at  $\theta = 45^\circ$  or less for specimens deformed at 500 bar or less confining pressure. Similar preferred orientations exist in photoelastic models with naturally shaped elements (Fig. 29c, 29d). For specimens deformed at 1,000 bar confining pressure the frequency of chains is more uniform from  $\theta$  values of  $0-90^\circ$ .



Fig. 32. Fractures in a quartz grain of St. Peter Sand which result from a triple load. (Experiment 450, Table III.) Center grain is 0.25 mm in diameter.

Contact lines for experimentally deformed quartz sand are more or less uniformly oriented at  $\theta$  angles from 0 to  $90^\circ$  much like those in photoelastic models with naturally shaped elements (Fig. 29a, 30a). These models also predict that microfractures in analogous granular materials will have preferred orientations for  $\theta$  less than  $45^\circ$  (Fig. 29b, 30b). Microfracture orientations in experimentally deformed St. Peter Sand confirm this prediction (Fig. 34). Similar preferred angular relations have been noted for rocks by other workers (e.g., Friedman, 1963; Hoshino and Koide, 1970).

#### *Cemented aggregates*

Since clastic sedimentary rocks are natural aggregates of grains that are all cemented to some degree, this study of microfracturing would be incomplete without consideration of

the role of cementation. Moreover, an explanation is needed for the fact that micro-fracture orientation patterns in cemented sandstones are invariably more highly ordered than are those in loose sands (Friedman, 1963).

The effects of cement on the states of stress in aggregates are examined for several different models of discs and naturally shaped elements of both CR-39 and PSM-1. The cementing process itself introduces small stresses into photoelastic discs. The stress difference, caused by the contraction of the cement during curing, is less than 10 bar, and it can be neglected. In aggregates cemented while not under load, subsequent boundary loads are transmitted from grain to grain as in uncemented aggregates although some of the applied load is transmitted by the cement and rigid-body movements of grains before and after fracture are inhibited. In aggregates cemented while under load, the locked-in



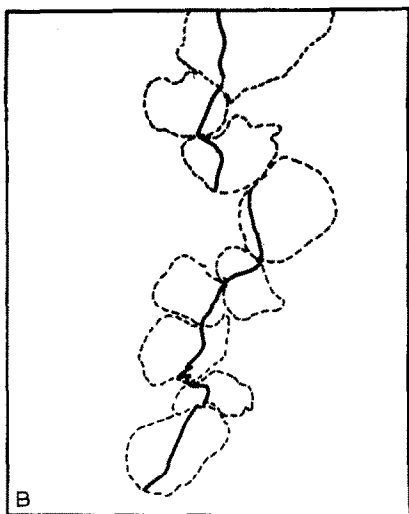


Fig. 33. Microfracture chains in quartz grains of St. Peter Sand deformed at 1,000 bar confining pressure. These grains are from experiment 450 (Table III). The dashed lines in (B) represent tracings of grain boundaries in (A). Similarly, solid lines in (B) are microfractures that form chains in (A). Note that most of the basic fracture patterns predicted from photoelastic study of naturally shaped elements (Fig. 28) can be recognized in these sand grains.

elastic strains further influence the subsequent mechanical behavior of the aggregate (Friedman and Logan, 1970).

When the cemented models are loaded externally, the stress patterns observed in the discs are much more uniform than are those in uncemented models. The stress distributions are especially uniform when the loading bars are in contact with the cement only (Fig. 35). That is, the relative importance of disc contacts as stress risers is significantly reduced. The highest maximum stress differences in uncemented aggregates are in small regions very close to contacts, but in cemented aggregates they cover broad regions in the central sectors of the discs. Moreover, the trajectories of the principal stresses in the

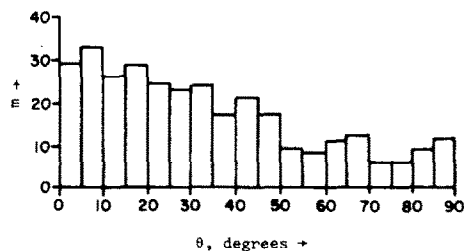


Fig. 34. Histogram showing  $m$  as a function of  $\theta$  for mixed quartz grain sizes of St. Peter Sand deformed at 350 bar confining pressure. Note that without contact-line data it is more difficult to interpret microfracture orientations. Contact lines are more or less uniformly distributed. (Experiment 12, Table II.)

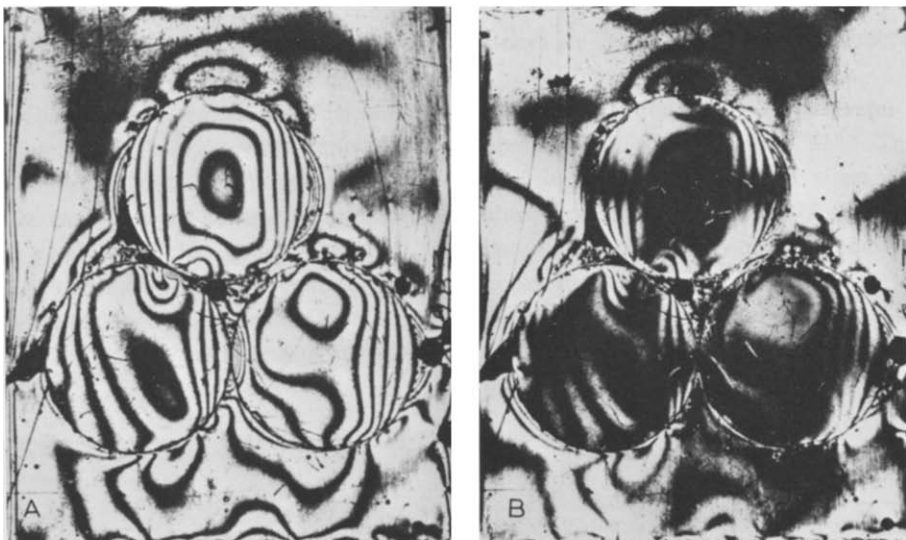


Fig. 35. Photoelastic patterns for a cemented, three-disc model. Discs of PSM-1 are cemented with CIBA epoxy. Vertical load is applied to the cement. Discs are 1.5 cm diameter and 0.6 cm thick. Isochromatic fringes originate in central area of discs not near the contacts as in uncemented models (A). Isoclinics are very broad and not well defined (B). The cement is also stressed, but no analysis is attempted.

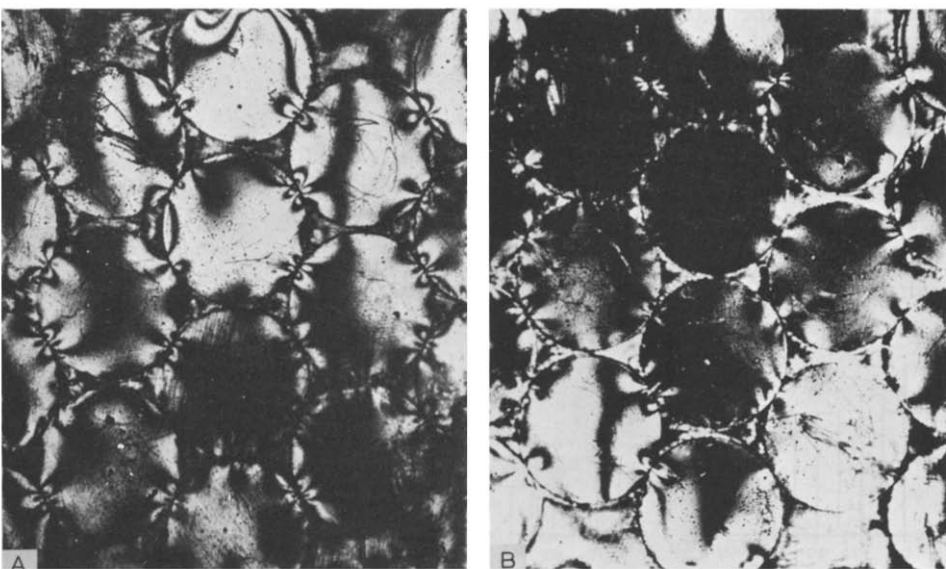


Fig. 36. Photoelastic patterns for a cemented, many-disc model. Discs of PSM-1 are cemented with CIBA epoxy. Vertical load is applied to both cement and discs. Discs are same size as in Fig. 35. Isochromatic fringes are broadly distributed through discs and cement and are only slightly influenced by the disc contacts (A). Isoclinics defining vertical and horizontal principal stress are also broad and show that in many of the discs the principal stresses are uniformly oriented parallel to the external load (B).

central regions of the discs are uniformly subparallel to the load axes across the boundaries of the aggregate as a whole. When the loading bars are in contact with both cement and discs, stress concentrations at disc contacts are slightly more pronounced than in discs immersed in cement (Fig. 36).

Recall that in uncemented aggregates grain contacts act as important stress risers, so that fracturing along lines between contacts tends to occur, and fracture orientations depend strongly on the positioning of critical contacts as well as the directions of applied loads. Fractures tend to lie between  $0^\circ$  and  $45^\circ$  to  $P_1$ . In cemented aggregates, on the other hand, the stress distribution is much more uniform, and fractures should tend to form at nearly  $90^\circ$  to the least principal stress ( $\sigma_3$ ) across the boundaries of the aggregate in bulk, and independently of the detailed grain-contact geometry.

## DISCUSSION

The mechanical behavior of granular aggregates is not as yet completely understood, but the present work has clarified several aspects of the problem, especially the relation of states of stress in grains to microfracturing and both, in turn, to the grain shape, packing, sorting and cementing characteristics of the aggregate and the direction and relative magnitudes of the loads at the boundaries of the aggregate.

### *Basic states of stress in grains*

Analysis of two-dimensional states of stress in cemented and uncemented photo-mechanical models reveals six different states for individual naturally shaped elements (Fig. 27). Which one of these basic states exists in a loaded sand grain depends most importantly on the intensity of forces applied at grain contacts, and both the number and distribution of contacts on the grain. Those factors depend in turn on the load conditions at the boundaries of the aggregate and the characteristics of the aggregate itself, especially packing arrangement, size, sorting, and cement. If states of stress in grains within natural aggregates under load could be determined, then it would be possible to reconstruct the orientations and the relative magnitudes of boundary loads in addition to the initial packing and the sorting characteristics of the aggregate. States of stress cannot be determined directly, but microfracture data make such reconstructions possible.

### *Extension-fracture criterion*

Previous workers found that microfracture orientations in both cemented and uncemented sand aggregates bore a definite relation to the axis of greatest load (Borg et al., 1960; Friedman, 1963; Hoshino and Koide, 1970). It was assumed that within some small domain, for example of the size of the usual triaxial specimen (Friedman and Sowers, 1970, p.481), the type of microfracture, whether shear or extension, could be identified

by its angular relation to  $P_1$ . This assumption is valid for nearly isotropic rocks, but requires modification if it is to be applied to granular aggregates. In order to determine whether microfractures in a granular aggregate are of the shear or extension type, the relation of fractures to principal stresses within individual grains must be established. This has now been done, and microfractures follow  $\sigma_1$  trajectories in areas within individual grains where the maximum stress difference has its greatest value and are, therefore, extension microfractures. This empirically established relation between stress and fracturing, designated as the extension-fracture criterion, makes possible new interpretations of fracture patterns in grains and microfracture fabrics of aggregates.

### *Fracture patterns in grains*

Photoelastic study predicts that fractures due to single loads (Fig. 28a) should occur more frequently than those due to any of the other basic load configurations. However, only a very few fractures of this type are recognized in experimentally deformed glass beads and quartz sand. Fractures that form at the low-magnitude concentrations at single-load points, tend to become stable a short distance into the grain and they are not likely to penetrate the grain (Fig. 28a). This sort of stability is similar to that observed for cracks in compression (Brace and Bombolakis, 1963). Fractures associated with the other basic load conditions are more likely to cut through grains because an area of high maximum stress difference connects critical contacts (Fig. 27, 28).

Indeed, fracture patterns observed in deformed glass beads and quartz sand grains bear strong resemblances to predicted patterns. Examination of thin sections shows that fractures due to diametral and triple loads predominate at 350 bar confining pressure, but they become rarer as confining pressure increases beyond 500 bar. Complex patterns due to combined loads are more frequent at 1,000 bar, but they are uncommon at lower pressures. The quadruple-load fracture pattern is common at least up to 1,000 bar. Fractures apparently due to diametral, triple, quadruple and combined loads were observed in thin sections of naturally deformed sand obtained from R.R. Berg (personal communication, 1971). These comparisons suggest that the extension-fracture criterion applies to naturally deformed aggregates.

### *Chains of microfractures*

For ideally packed circular discs, photoelastic observations combined with the extension-fracture criterion indicate that microfracture chains can exist and ought to have the same orientations as concentrations of microfractures predicted from photoelastic data (Fig. 14, 16, 17). The reason for chain development is that the average maximum stress difference along series of contact lines at small angles to  $P_1$  is significantly higher than along lines with greater  $\theta$  values. In a typical photoelastic model of discs the average value for the maximum stress difference along chains of contact lines with  $\theta$  values of  $0^\circ$  or  $30^\circ$  is one fringe, while the fringe order on lines at  $60^\circ$  or  $90^\circ$  is less than one half. The

photoelastic data on chains are confirmed by observations of chains of microfracture at small angles to  $P_1$  in experimentally deformed glass beads (Fig. 21c).

Similar chains are observed in photoelastic models with naturally shaped elements in which a certain series of discs may be more highly stressed than any other. Such chains tend to be oriented at a low angle to the direction of greatest load. In the light of the extension-fracture criterion, this fact leads to the prediction that chains of fracture ought to occur in sand grains, also at small angles to the direction of maximum compression. This prediction is confirmed by observations of chains of microfracture at low  $\theta$  angles in experimentally deformed St. Peter Sand (Fig. 33).

Chain development in uncemented aggregates at about 6% strain and confining pressures of about 350 bar is not conspicuous. Once fracture occurs in one grain of a highly stressed series the intensity of stress is reduced locally; and most broken grains are free of constraint and are able to rotate into pore spaces. At higher confining pressures near 1,000 bar or at shortenings near 15%, grains are more likely to be constrained by crushed material, and conditions are more favorable for chain development.

Chains of microfracture occur in the thin sections of naturally deformed sand supplied by R.R. Berg. Some of these chains involve ten or more grains. It is noteworthy that fragments from demolished grains are abundant.

#### *Stress concentrations and fractures near grain contacts*

The tendency for fractures to join into chains is inhibited by small changes in the state of stress at grain contacts. Near contacts, maximum stress difference is very high and, intuitively, fracturing would seem more likely to start there than anywhere else in a grain. This supposition is supported by theory. In general, elastic bodies deform at contacts and touch one another on one or more very small surface areas. For spheres, the Hertzian analytical solution (e.g., Love, 1944, p.193) predicts contact on a very small annular area, and this has been verified in experiments on glass spheres by Mindlin et al. (1951). The presence of concentrations near contacts of spheres results from this small contact area.

Similarly, the edge of a disc in contact with a flat plate is loaded over a small area (Fairhurst, 1964), and stress concentrations occur near both edges of contact. The resulting contact is, in effect, two elongate rectangular (or strip) loads placed very close together. The resultant concentration is due to the interaction of the states of stress that result from these small area loads (Jessop and Harris, 1949, p.133). The stress distribution for this case was studied analytically by Poritsky (1950), and the lines of maximum stress difference he derived are essentially the same as those reflected by the fringes depicted in Fig. 37A.

Comparison of photoelastic and fracture data for rock discs shows that the small fractures which form inside the U-shaped area near contacts (Fig. 37B) seem to follow the line connecting points of greatest curvature of isostatics of maximum stress difference in just those regions where stress trajectories are poorly known. Whether these fractures are of the shear or extension type is not known. Some workers have interpreted them as

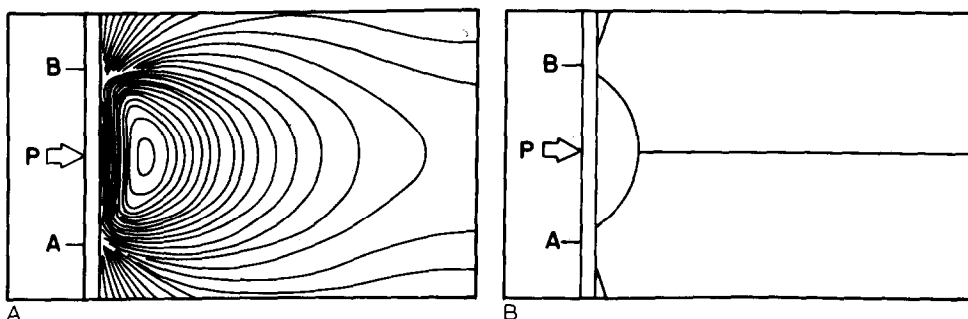


Fig. 37. Detail at a contact between a circular disc and a plane surface. A. Fringes near the contact (after Durelli and Riley, 1965, p.45). The closed elliptical isochromatic to the right of  $P$  has a fringe order of 27. B. Fracture pattern expected by application of a slightly modified extension-fracture criterion to photoelastic data. The contact between the plane and the disc extends from  $A$  to  $B$ . Load  $P$  is applied in the direction shown by a load bar. Where fringes are very close together in the vicinity of  $A$  and  $B$  they are omitted.

shear fractures for two reasons: (1) fractures occur at acute angles of about  $30^\circ$  to the greatest load direction (assumed to be also the  $\sigma_1$ -axis), the usual position for shear fractures; and (2) crushed material is observed on the fracture surfaces.

The first reason is based on the idealized solution for the state of stress in a disc in contact with a plane which can be found in most standard engineering texts on elasticity (e.g., Timoshenko and Goodier, 1970). Actually, this solution must be extrapolated into the small region near contacts, and most experimentalists do not attempt this (e.g., Frocht, 1948, p.145; Jessop and Harris, 1949, p.135). Some doubts have been expressed about the applicability of theoretical solutions to fracturing, specifically because of changes of stresses near contacts (Fairhurst, 1964, p.536). Nevertheless, idealized solutions are used in conjunction with standard criteria for fracture, like shear failure at angles  $\leq 45^\circ$  to  $\sigma_1$ . However, because the state of stress near contacts is poorly known, it is equally probable that these fractures follow  $\sigma_1$  trajectories in areas of locally greatest maximum stress difference and that they are, in fact, extension fractures.

The second reason is also subject to question. Consider, as a possible alternative explanation, the following sequence of events: fractures near contacts form where maximum stress difference is highest in the disc. They form and take on the shape of a wedge or cone. The wedge or cone is then pushed into the unfractured portion of the grain. At this time sliding of irregular wedge- or cone-shaped fracture surfaces grinds up the material. The wedge then contributes to throughgoing fracture by enhancing the existing critical state of extension across a contact line.

This discussion is one example of how photomechanics can provide insight toward the solution of a problem in rock mechanics. Moreover, a further photomechanical study in much greater detail would probably reveal whether fractures in regions near contacts are in fact of the extension or shear type.

### *Orientation of contact lines and microfractures in the uncemented granular aggregates*

Certain trends are of potential value for interpretations of the conditions under which natural aggregates were deformed. The most apparent is the tendency for microfractures to be oriented subparallel to the direction of greatest boundary compressive load and to cluster at other orientations that depend on the size sorting, dominant grain shape and packing arrangement of the aggregate.

Contact lines are more randomly oriented than microfractures, i.e., their frequency is more uniform for all  $\theta$  values. Nevertheless, they show peaks that are influenced by the packing, sorting and grain-shape characteristics of the aggregate, and they are most helpful for interpreting concentrations of microfractures.

Confining pressure can enhance or diminish the effects of packing, sorting and grain-shape on microfracture orientations. Aggregates that are well-sorted, or that consist uniformly of nearly spherical grains, or that are deformed at low confining pressures (less than about 350 bar), show packing effects more strongly than those that are poorly sorted, that have less regularly shaped grains, or that are deformed at high confining pressures (circa 1,000 bar).

For naturally deformed aggregates it ought to be possible to reconstruct the direction in which the greatest load acted across their boundaries from microfracture and contact-line orientation data. If, in addition, size sorting and grain shape are evaluated, even if qualitatively, it should be possible to reconstruct the dominant packing arrangement and relative intensity (i.e., whether high or low) of confining pressure as well. Reconstructions of this type have potential value in improving permeability estimates by methods like those used by Berg (1970).

### *Microfractures and microfracture chains in cemented aggregates*

When loads are applied to cemented models which are simple analogs of cemented sandstones, stress distributions are more uniform not only in individual grains but also for the aggregate as a whole. Together with the extension-fracture criterion, this observation suggests that microfractures would tend to form in parallel sets and that these sets would be strongly oriented subparallel to the maximum compressive load across the boundaries of the aggregate. This prediction agrees with published observations of microfracture patterns in cemented as compared with uncemented sands (Friedman, 1963, pp.20–25; Borg et al., 1960, p.172, respectively). This prediction is further supported by the orientation data for individual microfractures in cemented sandstone presented herein (Fig. 38).

It is also apparent that as the influence of the cement on the orientations of microfractures increases, the influences of packing, sorting, shape, and confining pressure are reduced, especially in comparison with uncemented aggregates. For example, Moore (1970) shows that uncemented sands reach densest packing (rhombohedral) i.e., 26%, at a depth of burial of about 6,000 ft. The presence of calcite cement kept grains from densest packing until the rock was buried at a depth of about 18,000 ft.

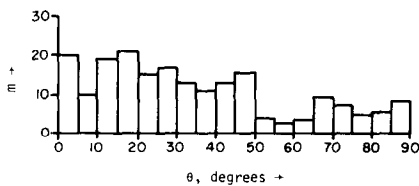


Fig. 38. Histogram showing  $m$  in quartz grains of experimentally deformed Coconino Sandstone as a function of  $\theta$ . Specimen HS-54 (Swolfs and Logan, 1970) shortened 3.2% at 1 kbar confining pressure, 0.5 kbar pore water pressure, 200° C. Note that fractures in plane of thin section tend to be at angles  $\theta$  of less than 50°.

Chains of microfracture are expected to be more common in cemented than in uncemented aggregates because in the former grains are constrained and states of stress are more uniform from grain to grain. Constraint enhances chain development because fragments of fractured grains cannot rotate into voids. The state of stress in a series of highly stressed grains is probably not much relieved when one grain in the chain fractures; in fact the differential stresses may be enhanced if a sharp edge of the fractured grain causes a high stress concentration where it contacts its neighbor.

The prediction that chains of microfracture ought to be more common in cemented aggregates leads to the interesting speculation that such chains may play an important role in the macroscopic fracture of granular aggregates. The chains might act as unstable flaws (Griffith flaws), and propagate through the aggregate when a critical length is exceeded. Even though the chains are composed of extension microfractures, the chains frequently are inclined to  $\sigma_1$  across the boundaries of the aggregate. Such chains would then propagate and lead to macroscopic shear fracture. In any event, microfracture chains have been observed, and an investigation of the relation between such chains and macrofracturing would be an important further extension of this work on granular aggregates.

## CONCLUSIONS

The following conclusions about the deformations of granular aggregates seem warranted:

- (1) Most, if not all, fractures within individual quartz grains (microfractures) are extension fractures that follow critical contact lines.
- (2) Microfracture and contact-line orientations are related to the orientations and relative magnitudes of boundary loads and to the packing arrangement, size sorting, and dominant grain shapes in the aggregate.
- (3) Some microfractures tend to join together in chains that are frequently oriented at small angles to the direction of the greatest boundary load.
- (4) Microfracture orientations are more uniform for cemented aggregates than for uncemented aggregates.

## ACKNOWLEDGMENTS

Our gratitude is extended to F.A. Donath for his critical review of the manuscript.

We thank A.F. Gangi, J.M. Logan, W.Z. Savage, D.W. Stearns, and H.S. Swolfs for helpful discussions during the course of the work.

This research was generously sponsored by Advance Research Projects Agency. Contract number DACA 73-68-C-0004.

## REFERENCES

- Arbiter, N., Harris, C.C. and Stamboltzis, G., 1968. Single fracture of brittle spheres. *Soc. Min. Eng., Prepr.*, 68-B-83, 39 p.
- Berg, R.R., 1970. Method for determining permeability from reservoir rock properties. *Gulf Coast Assoc. Geol. Soc., Trans.*, 20: 303-317.
- Bloss, D.F., 1964. Anisotropy of fracture in quartz. *Am. J. Sci.*, 255: 214-226.
- Bombolakis, E.G., 1964. Photoelastic investigation of brittle crack growth within a field of uniaxial compression. *Tectonophysics*, 1: 343-351.
- Borg, I. and Maxwell, J.C., 1956. Interpretation of fabrics of experimentally deformed sands. *Am. J. Sci.*, 254: 71-81.
- Borg, I., Friedman, M., Handin, J. and Higgs, D.V., 1960. Experimental deformation of St. Peter Sand: A study of cataclastic flow. In: D. Griggs and J. Handin (Editors), *Rock Deformation, A Symposium*. Geol. Soc. Am., New York, N.Y., pp. 133-191.
- Brace, W.F. and Bombolakis, E.G., 1963. A note on brittle crack growth in compression. *J. Geophys. Res.*, 68: 3709-3714.
- Brace, W.F., Paulding, Jr., B.W. and Scholz, C.H., 1966. Dilatancy in the fracture of crystalline rocks. *J. Geophys. Res.*, 71: 3939-3953.
- Coker, E. and Filon, L., 1931. *A Treatise on Photoelasticity*. Cambridge University Press, London, 720 p.
- Dantu, P., 1968. Etude statistique des forces intergranulaires dans un milieu pulvérulent. *Geotechnique*, 18: 50-55.
- Durelli, A.J. and Riley, W.F., 1965. *Introduction to Photomechanics*. Prentice-Hall, Englewood Cliffs, N.J., 402 p.
- Durrance, E.M., 1969. Release of strain energy as a mechanism for the mechanical weathering of granular rock material. *Geol. Mag.*, 106: 496-497.
- Fairhurst, C., 1964. On the validity of the "Brazilian" test for brittle materials. *Int. J. Rock Mech. and Min. Sci.*, 1: 535-546.
- Friedman, M., 1963. Petrofabric analysis of experimentally deformed calcite-cemented sandstones. *J. Geol.*, 71: 12-37.
- Friedman, M., 1964. Petrofabric techniques for the determination of principal stress directions in rocks. In: W.R. Iudd (Editor), *State of Stress in the Earth's Crust*. Elsevier, New York, N.Y., pp. 451-552.
- Friedman, M., 1967. Measurement of the state of residual elastic strain in rocks by X-ray diffractometry. *Norelco Rep.*, 14: 7-9.
- Friedman, M., 1968. X-ray analysis of residual elastic strains in quartzose rocks. In: K.E. Gray (Editor), *Proc. Symp. Rock Mech., 10th, Univ. Texas, Austin, Texas*.
- Friedman, M. and Logan, J.M., 1970. The influence of residual elastic strain on the orientation of experimental fractures in three quartzose sandstones. *J. Geophys. Res.*, 75: 387-405.
- Friedman, M. and Sowers, G.M., 1970. Petrofabrics: A critical review. *Can. J. Earth Sci.*, 7: 477-497.
- Friedman, M., Perkins, R.D. and Green, S.J., 1970. Observation of brittle-deformation features at the maximum stress of Westerly Granite and Solnhofen Limestone. *Int. J. Rock Mech. Min. Sci.*, 7: 297-306.

- Frocht, M.M., 1941. *Photoelasticity*, 1. Wiley, New York, N.Y., 411 p.
- Frocht, M.M., 1948. *Photoelasticity*, 2. Wiley, New York, N.Y., 505 p.
- Fuchs, S., 1913. Hauptspannungstrajektorien bei der Beruehrung einer Kugel mit einer Platte. *Phys. Z.*, 14: 1282–1285.
- Gallagher, J.J., 1971. *Photomechanical Model Studies Relating to Fracture and Residual Elastic Strain in Granular Aggregates*. Thesis, Texas A and M Univ., College Station, Texas, 127 p.
- Gallagher, J.J., Sowers, G.M. and Friedman, M., 1970a. Photomechanical model studies relating to fracture in granular rock aggregates. *Geol. Soc. Am., Abstr.*, 2: 285.
- Gallagher, J.J., Sowers, G.M. and Friedman, M., 1970b. Photomechanical studies relating to fracture and stored stress in granular rock aggregates. *Can. Conf. Res. Tectonics, 3rd, Winnipeg, Man.*, 1970 (unpublished).
- Geertsma, J., 1963. Photoelastic studies of the fallible behavior of granular materials. In: C. Fairhurst (Editor), *Rock Mechanics*. Pergamon Press, New York, N.Y., pp. 713–715.
- Graton, L.C. and Fraser, H.J., 1935. Systematic packing of spheres with particular relation to porosity and permeability. *J. Geol.*, 34: 785–904.
- Handin, J. and Griggs, D., 1951. Deformation of Yule Marble: Part II – Predicted fabric changes. *Bull. Geol. Soc. Am.*, 62: 863–886.
- Heard, H.C., 1963. Effect of large changes in strain rate in the experimental deformation of Yule Marble. *J. Geol.*, 71: 162–195.
- Hoshino, K. and Koido, H., 1970. Process of deformation of the sedimentary rocks. *Proc. Congr. Int. Soc. Rock Mech.*, 2nd, Belgrade, vol. 1, paper 2–13.
- Jaeger, J.C., 1964. *Elasticity, Fracture and Flow with Engineering and Geological Applications*. Wiley, New York, N.Y., 212 p.
- Jaeger, J.C., 1966. Brittle fracture of rocks. In: C. Fairhurst (Editor), *Failure and Breakage of Rock*. American Institute of Mining Engineers, New York, N.Y., pp. 3–57.
- Jessop, H.T. and Harris, F.C., 1949. *Photoelasticity, Principles and Methods*. Cleaver-Hume Press Ltd., London, 184 p.
- Lee, K.L. and Farhoomand, I., 1967. Compressibility and crushing of granular soil in anisotropic triaxial compression. *Can. Geotech. J.*, 4: 68–99.
- Love, A.E.H., 1944. *A Treatise on the Mathematical Theory of Elasticity*. Dover, New York, N.Y., 643 p.
- Miller, E.T., 1963. The response of soils to dynamic loading. *M.I.T., Dep. Civ. Eng. Publ.*, R63–39.
- Mindlin, R.D., 1949. Compliance of elastic bodies in contact. *J. Appl. Mech.*, 71: 259–268.
- Mindlin, R.D., 1954. Mechanics of granular media. In: P.M. Naghdi (Editor), *Proc. U.S. Natl. Congr. Applied Mech.*, 2nd, Ann Arbor, Mich., pp. 13–20.
- Mindlin, R.D., Mason, W.P., Osmer, T.F. and Deresiewicz, H., 1951. Effects of an oscillating tangential force on the contact of surfaces of elastic spheres. In: E. Sternberg (Editor), *Proc. U.S. Natl. Congr. Applied Mech.*, 1st, Chicago, Ill., pp. 203–208.
- Moore, W.R., 1970. *Sedimentary History of the Casper Formation (Wolfcampian), Powder River Basin, Wyoming*. Thesis Texas A and M Univ., College Station, Texas.
- Photoelastic Incorporated, 1970. Photoelastic coating and model materials. *Photoelastic Inc., Bull.*, P–1120, 8 p.
- Poritsky, H., 1950. Stresses and deflections of cylindrical bodies in contact with application to contact of gears and locomotive wheels. *J. Appl. Mech.*, 17: 191–201.
- Price, N.J., 1966. *Fault and Joint Development in Brittle and Semibrittle Rocks*. Pergamon Press, Oxford, 172 p.
- Ramsay, J.G., 1967. *Folding and Fracture of Rocks*. McGraw-Hill, New York, N.Y., 568 p.
- Rowe, P.W., 1962. The stress-dilatancy relation for static equilibrium of an assembly of particles in contact. *Proc. R. Soc. London, Ser. A*, 269: 500–527.
- Rowe, P.W., 1964. Energy components during the triaxial cell and direct shear tests. *Geotechnique*, 14: 247–261.
- Scholz, C.H., 1968a. Microfracturing and the inelastic deformation of rocks in compression. *J. Geophys. Res.*, 73: 1417–1432.
- Scholz, C.H., 1968b. Experimental study of the fracturing process in brittle rocks. *J. Geophys. Res.*, 73: 1447–1454.

- Swolfs, H.S. and Logan, J.M., 1970. Experimental evidence of the role of pore fluid chemistry on the mechanism of fracture in sandstone. *Geol. Soc. Am., Abstr.*, 2: 699.
- Timoshenko, S.P. and Goodier, J.N., 1970. *Theory of Elasticity*. McGraw-Hill, New York, N.Y., 567 p.
- Trollope, D.H., 1968. The mechanics of discontinua or clastic mechanics in rock problems. In: K. S. Stagg and O.C. Zienkiewicz (Editors), *Rock Mechanics in Engineering Practice*. Wiley, New York, N.Y., pp. 275–317.
- Weber, J., 1968. Etude théorique et expérimentale de la similitude, dans les essais sur modèles du comportement mécanique des milieux granulaires. *Ann. Ponts Chaussées*, 138: 25–34.
- Whitman, R.U., 1963. Comments regarding significance of the theoretical results: Stresses and strains in a planar array of elastic spheres. *M.I.T., Dep. Civ. Eng. Publ.*, R63–39, pp. A1–A5.